Deeply gapped vegetation patterns: On crown/root allometry, criticality and desertification

R. René Lefever, Nicolas Barbier, Pierre Couteron, Olivier Lejeune

www.elsevier.com/locate/yjtbi

Deeply gapped vegetation patterns: On crown/root allometry, criticality and desertification

René Lefever, Nicolas Barbier, Pierre Couteron, Olivier Lejeune

PII: S0022-5193(09)00342-7
DOI: doi:10.1016/j.jtbi.2009.07.030
Reference: YJTBI 5647

To appear in: *Journal of Theoretical Biology*

Received date: 22 November 2008
Revised date: 14 July 2009
Accepted date: 23 July 2009

Cite this article as: René Lefever, Nicolas Barbier, Pierre Couteron and Olivier Lejeune, Deeply gapped vegetation patterns: On crown/root allometry, criticality and desertification, *Journal of Theoretical Biology*, doi:10.1016/j.jtbi.2009.07.030

Deeply gapped vegetation patterns: on crown/root allometry, criticality and desertification

René Lefever [a], Nicolas Barbier [b,c], Pierre Couteron [c], Olivier Lejeune [a]

[a] *Service de Chimie Physique et Biologie Théorique, Université Libre de Bruxelles CP 231, B-1050 Bruxelles, Belgium*
[b] *Service de Complexité et Dynamique des Systèmes Tropicaux, Université Libre de Bruxelles CP 169, B-1050 Bruxelles, Belgium*
[c] *IRD-UMR Botanique et Bioinformatique de l'Architecture des Plantes (AMAP), Boulevard de la Lironde, 34398 Montpellier Cedex 05, France*

Abstract

The dynamics of vegetation is formulated in terms of the allometric and structural properties of plants. Within the framework of a general and yet parsimonious approach, we focus on the relationship between the morphology of individual plants and the spatial organization of vegetation populations. So far, in theoretical as well as in field studies, this relationship has received only scant attention. The results reported remedy to this shortcoming. They highlight the importance of the crown/root ratio and demonstrate that the allometric relationship between this ratio and plant development plays an essential part in all matters regarding ecosystems stability under conditions of limited soil (water) resources. This allometry determines the coordinates in parameter space of a critical point that controls the conditions in which the emergence of self-organized biomass distributions is possible. We have quantified this relationship in terms of parameters that are accessible by measurement of individual plant characteristics. It is further demonstrated that, close to criticality, the dynamics of plant populations is given by a variational Swift-Hohenberg equation. The evolution of vegetation in response to increasing aridity, the conditions of gapped pattern formation and the conditions under which desertification takes place are investigated more specifically. It is shown that desertification may occur either as a *local desertification process* that does not affect pattern morphology in the course of its unfolding or as a *gap coarsening process* after the emergence of a transitory, deeply gapped pattern regime. Our results amend the commonly held interpretation associating vegetation patterns with a Turing instability. They provide a more unified understanding of vegetation self-organization within the broad context of matter order-disorder transitions.

Key words: vegetation gapped patterns, competition, self-organization, diffusion instability in ecosystems, Swift-Hohenberg equation.

1. Introduction

Many regions exhibit landscapes whose vegetation cover consists of a regular distribution of densely vegetated areas and zones of bare soil (see *e.g.*, Valentin and Poesen, 1999; Tongway *et al.*, 2001; Couteron, 2002; Deblauwe *et al.*, 2008). These landscapes, of which Fig. 1*a* is an example, are mainly found in climates where the potential evapotranspiration substantially exceeds the mean annual precipitation. The natural formation of these large ecological organizations can be explained by this hydric stress combined with redistribution and conservation mechanisms that allocate more limiting resources, water in particular, to vegetated patches than to bare soil (Schlesinger *et al.*, 1990; Wilcox *et al.*, 2003; Ludwig *et al.*, 2005; Breshears, 2006).
Several mathematical formulations of this explanation have been developed. In general, vegetation patterning is interpreted as a process of self-organization that takes shape via a non-equilibrium instability. This instability may either be a symmetry-breaking phenomenon in the strict sense, likely to take place even if the environment is isotropic (Lefever and Lejeune, 1997; HilleRis-Lambers *et al.*, 2001; von Hardenberg *et al.*, 2001; Shnerb *al.*, 2003; D'Odorico *et al.*, 2006; Kéfi, 2008), or it may be an advection-induced transition that requires the pre-existence of some environmental (usually topographical) anisotropy (Klausmeier, 1999; Okayasu and Aizawa, 2001; Sherratt, 2005;

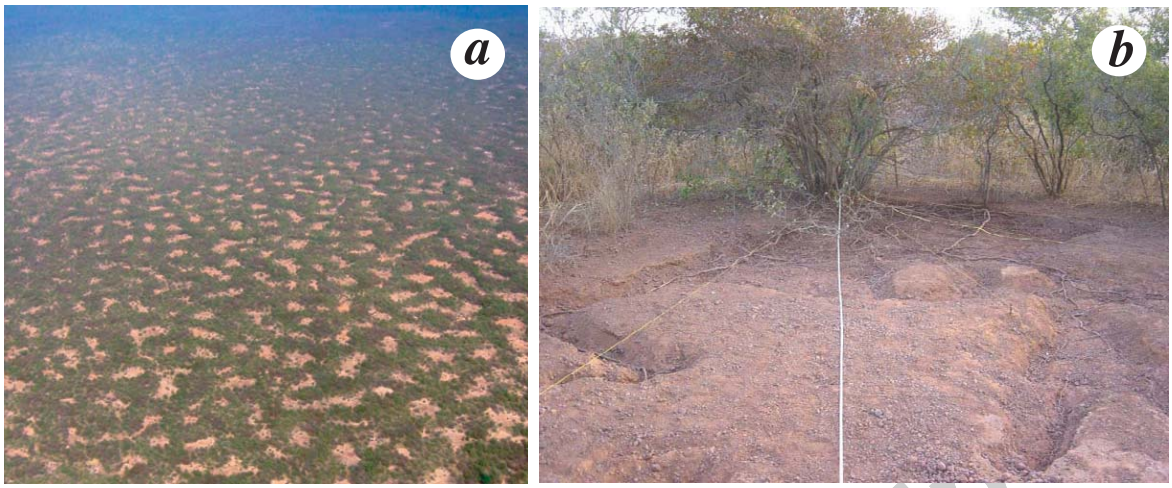

Fig. 1. (*a*) Sub-Sahelian gapped landscape dominated by the shrub species *Combretum micranthum* G. Don in South-West Niger. Shrub crown radius and bare spot distances are approximately 1.75 m and 50 m. (*b*) The rhizospheres of five shrubs were excavated. The normalized biovolume b of each shrub was computed as the ratio of its biovolume (*i.e.*, crown area times total height) to that of the largest individual. Values ranged between 0.1 and 1. Roots penetrated down to ca. 40-cm depth but their spread could exceed the crown radius by one order of magnitude. The best fits of Φ_c were obtained for an exponential function with $L_c^0 = 1.27$ and $p = 1/3$. Facilitation consisted of a drastic reduction of direct soil evaporation. Soil water sensors were used to parameterize Φ_f like Φ_c by an exponential. Attempts to fit with other functions did not yield substantially better fits. A clear optimum was found for $L_f^0 = 0.81$ (Barbier *et al.*, 2006, 2008).

Ursino, 2005). Recent campaigns of measurement in the field, notably in the sub-Sahelian territories of Niger, strongly support the hypothesis that the instability underlying the formation of gapped patterns (cf. Fig. 1a) is symmetry-breaking in the strict sense (Barbier, 2006; Barbier *et al.*, 2006, 2008). As such, this instability can occur in the absence of slope-induced water redistribution, a mechanism that has long been thought to be primordial for vegetation pattern formation (Tongway *et al.*, 2001). Gapped patterns are observed from Burkina Faso (Couteron and Lejeune, 2001) to Sudan (Deblauwe *et al.*, 2008). Besides their periodicity, they display a strong contrast (see Fig. 1a) between the gaps, where the biomass is close to zero, and the vegetated matrix where the vegetation may reach values of 12t/ha in Southern Niger (Hiernaux and Gérard, 1999).

So far, in theoretical studies as well as in field studies, the relationship between the elementary structure of individual plants and the collective organization of plant populations has received only scant attention. Our study is intended to clarify this relationship in light of the results obtained in recent campaigns of field measurement (Barbier, 2006; Barbier *et al.*, 2008). Using a similar approach to that adopted in our earlier works (Lefever and Lejeune, 1997; Lejeune *et al.*, 1999; Lefever *et al.*, 2000; Couteron and Lejeune, 2001; Lejeune *et al.*, 2004; Tlidi *et al.*, 2008), we aimed to achieve a general and yet parsimonious theoretical formulation explaining how the structure of individual plants shapes vegetation dynamics and how, as a consequence, vegetation may either adapt to varying environments or conversely collapse and become extinct (desertification).

It is well known that plants adapt their structures, especially their root structures (rhizosphere), to combat water scarcity (Schenk and Jackson, 2002; Barbier, 2006). When confronted with drought, they strive to increase their water resources by spreading their roots over a greater territory. Fig. 1*b* shows that in a shallow soil context, this lateral spread may extend beyond the radius of the aerial structure (crown) by an order of magnitude. In terms of morphological plasticity, this is an extraordinary achievement. However, whereas the lateral expansion of the roots allows for greater water uptake, it significantly increases the degree of *competition* between neighboring plants. As a consequence, it modifies the balance between competition and the positive feedback called *plant-plant facilitation*, which favors vegetation development in drylands(e.g. Callaway, 1995; Callaway *et al.*, 2003).

Understanding how such interactions operate at the scale of plant crown (for facilitation) and rhizosphere (for competition) to produce biomass organizations of landscape size is the main biological question studied in sections 2 to 4. The results highlight the role of the crown/root ratio which gives the relative size of the above-ground and below-ground structures. Furthermore, our results demonstrate that the allometric parameter linking plant development to this ratio plays an essential part in all matters regarding stability at the community level. Notably, this allometric parameter determines the coordinates in parameter space of a critical point that controls the feedback conditions for which an organization in the biomass distribution may emerge. We provide evidence for a fundamental link uniting criticality, vegetation patterning and plant morphology. We further demonstrate that close to their critical point, the dynamics of ecosystems is variational and can be described by a Swift-Hohenberg equation. Our results amend the current interpretation associating vegetation pattern formation with a Turing instability by providing a more unified understanding of vegetation self-organization within the broad context of matter order-disorder transitions. In section 5, we investigate more specifically the pathway of vegetation change in response to increasing aridity. We examine the conditions of gapped pattern formation and the conditions under which desertification takes place either as a *local desertification process* that does not affect patterns morphology in the course of its unfolding or as a *gaps coarsening process* that follows the emergence of a transitory deeply gapped pattern regime.

2. Vegetation interactions and crown-roots allometry

We consider a community within which, as shown in Fig. 1 and as it is often the case in drylands, a single species accounts for most of the biomass. Let L_a be the crown radial spread of the community's largest individual, $S = \pi L_a^2$ be a surface element centered on a point $\mathbf{r}$ and

$$\partial_t b(\mathbf{r},\, t) = b(\mathbf{r},\, t)\,[1 - b(\mathbf{r},\, t)]\;\mathcal{M}_f - \mu\, b(\mathbf{r},\, t)\mathcal{M}_c + \delta \int \Phi_D(|\mathbf{r}'|)\;[b(\mathbf{r}+\mathbf{r}',\, t) - b(\mathbf{r},\, t)\,]\; d\mathbf{r}' \qquad (1)$$

be the logistic equation governing the evolution of the biomass density $b(\mathbf{r},\, t)$ supported by this element at time t, normalized by the biomass density of the surface element S centered on the largest individual. The first two terms of (1) describe the biomass gains and losses; the third term models seed production, dispersion and germination; the logistic factor in the first term, $\big[1 - b(\mathbf{r},\, t)\big]$, expresses that $b(\mathbf{r},\, t) \in [0, 1]$. The time constants μ and δ are normalized with respect to the biomass doubling time and are thus dimensionless. They refer to individual (isolated) plants; more precisely, they represent the biomass loss/gain ratio and the ratio of biomass gains due to seeds and to growth. In the third term of (1), integration extends over the entire territory and space is normalized such that its unit be equal to L_a. The kernel of the integral is the Gaussian function

$$\Phi_D(|\mathbf{r}'|) = \frac{\sigma}{\pi} \exp\left(-\sigma\,|\mathbf{r}'|^2\right), \text{with } \sigma = \left(\frac{L_a}{L_d}\right)^2, \qquad (2)$$

weighting the seed flux decrease with distance according to the seed dispersion range L_d.

$\mathcal{M}_f$ and $\mathcal{M}_c$ are state functions that depend on the distribution of biomass around the surface element S centered on point $\mathbf{r}$. Their purpose is to model the facilitative and competitive interactions existing between plants and the dependence of these interactions upon plant development. $\mathcal{M}_f$ models interactions favoring vegetation development (facilitation) generated by the plant aerial structure. They involve the accumulation of nutrients in the neighborhood of the plants, the reciprocal sheltering of neighboring plants against climatic harshness, and the provision of shade, which improves the water budget in the soil (e.g. Callaway, 1995). The range L_f over which facilitation operates depends on the crown size. $\mathcal{M}_c$ models below-ground interactions involving rhizospheres. Plants confronted with drought develop large superficial root systems relative to their crown size in order to extract enough water from the topsoil (Schenk and Jackson, 2002). The range L_c of the competition generated by root systems depends on this extension (Callaway and Walker, 1997; Callaway *et al.*, 2002, 2003). Clearly, $\mathcal{M}_f$ and $\mathcal{M}_c$ must be positive definite functions of $b(\mathbf{r},\, t)$ taking values in the interval $[1, \infty)$ and must become equal to 1 in the limit where plants are too sparsely distributed to interact:

$$\lim_{b(\mathbf{r}+\mathbf{r}',\, t)\to 0} \mathcal{M}_\imath = 1, \quad (\imath = f, c). \qquad (3)$$

Hence, we assume that they are exponential functions whose argument is a mean field integral taken over the biomass distribution ($\imath = f, c$):

$$\mathcal{M}_\imath = \exp\left(\chi_\imath \int \Phi_\imath\ (|\mathbf{r}'|, L_\imath)\ b(\mathbf{r}+\mathbf{r}',\, t)\, d\mathbf{r}'\right). \quad (4)$$

Their kernels, given by

$$\Phi_\imath\ (|\mathbf{r}'|, L_\imath) = \mathcal{N}_\imath^{-1} \exp\left[-\frac{|\mathbf{r}'|}{L_\imath}\right], \quad (5)$$

describe how interactions vary with distance and plant development. To account for these dependencies, we set

$$L_\imath = L_\imath^0\, b(\mathbf{r}+\mathbf{r}',\, t)^p, \quad (6)$$

and define the norm $\mathcal{N}_\imath$ of (5) as

$$\mathcal{N}_\imath = \int \exp\left[-\frac{|\mathbf{r}|}{L_\imath^0}\right] d\mathbf{r}. \quad (7)$$

The exponent p and the constants L_f^0 and L_c^0 can be evaluated by field measurements of the crown and rhizosphere morphology (Barbier *et al.*, 2008). The allometric relation (6) allows us to avoid the complication of having to introduce more variables in order to describe the age classes of the community. It expresses that fully grown (mature) plants that produce significant feedback effects are unlikely to be present on a surface element S, centered on $\mathbf{r}+\mathbf{r}'$, if its biomass density $b(\mathbf{r}+\mathbf{r}',\, t)$ tends to zero. The contribution of such elements in the integral argument of (4) is negligible if p is a finite (non-zero) positive number. A similar relation, with $p=2$, has been used by Gilad *et al.*, (2004), Meron *et al.* (2007) and Sheffer *et al.* (2007). These authors however adopt another normalization condition and introduce a finite lower bound below which the range of interactions cannot decrease. We shall not adopt this assumption, which in our view is unnecessary. The parameters χ_f, χ_c model the interaction's strength; they depend on conditions such as soil nature and moisture index (quantified by the ratio of annual precipitation to potential evapotranspiration). Let us also define the *structural ratio*

$$\varepsilon \equiv \left(\frac{L_f^0}{L_c^0}\right)^2. \quad (8)$$

Use of the square power is motivated by the fact that hereafter only the square of L_f^0/L_c^0 appears in mathematical expressions. Together with the allometric parameter p, the structural ratio ε plays an important role in estimating the feedback strengths χ_f, χ_c and in predicting the wavelength of periodic patterns.

Finally, with respect to the modeling of plant interactions, let us point out that the field data gathered so far bear out expressions (5-7). For the ecosystem shown in Fig. 1, which is our reference example, the structure and development of the crown and rhizosphere of *Combretum micranthum* nicely fit with the assumption that interactions decrease exponentially with distance. The values of the parameters are (Barbier *et al.*, 2008):

$$p \approx 1/3,\ L_f^0 \approx 0.81\, L_a,\ L_c^0 \approx 1.27\, L_a. \quad (9)$$

For the structural ratio estimate, this yields:

$$\varepsilon \approx 0.41. \quad (10)$$

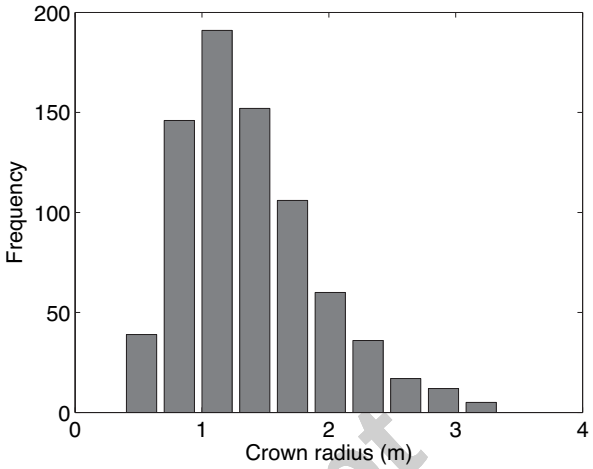

Fig. 2. Crown radius histogram: number of plants as a function of crown size for 750 individuals of C. micranthum above 1.5 m height measured in a plot of 0.4 ha representative of the Niger site seen in Fig. 1.

Fig. 2 reports a histogram of the crown radii established on the basis of measurements made for 750 individual plants constitutive of the pattern shown in Fig. 1a. Note that while the wavelength of this pattern (mean distance between bare spots) is

$$\lambda \approx 50 \text{ m}, \quad (11)$$

the maximum crown radius measured in the sampling for the most developed trees is

$$L_a \approx 3.25 \text{ m}. \quad (12)$$

3. Uniform stationary vegetation covers

3.1. *Plant development and vegetation critical point*

How age classes having different structural and functional potentialities influence the stability of vegetation has not been extensively studied. Nevertheless, it is generally recognized that plant-plant inter-

actions depend on development and that this relationship influences the biomass distribution. In our modeling, the allometric relation (6) and the normalization condition (7) express this relationship. It is shown in this section that their introduction allows us to predict the existence of a plait point (Korteweg, 1891) (referred to as a *critical point* from here forward). This prediction modifies the usual (mean field) stability diagrams of vegetation; it significantly improves their reliability at low biomass densities, a situation frequent in drylands.

Putting $b(\mathbf{r},\, t) = b(\mathbf{r}+\mathbf{r}',\, t) = b(t)$ transforms (1) into a simple logistic equation:

$$\frac{d\,b(t)}{d\,t} = e^{\chi_f\, b(t)^{(1+2\,p)}} \times \left[b(t)(1-b(t)) - \mu\, b(t) e^{\Lambda\, b(t)^{(1+2\,p)}}\right]. \tag{13}$$

Its stationary states, representing uniform vegetation cover, are the bare soil state $b_0 = 0$ and the curve $b_s \in [0,1]$ solution of

$$(1-b_s) - \mu \exp\left[-\Lambda\, b_s^{(1+2\,p)}\right] = 0. \tag{14}$$

The feedback difference

$$\Lambda \equiv \chi_f - \chi_c \tag{15}$$

measures the community *cooperativity* or *anti-cooperativity* according to whether it is positive or negative. If plants are too sparsely distributed to interact, or if facilitation and competition cancel each other out, $\Lambda = 0$. It is noteworthy that Eq. (13) is independent from the interaction ranges L_f and L_c. The normalization condition (7) has been chosen so that this mean field property can be recovered.

The stationary states of (13) are plotted in terms of μ for $p = 0$ in Fig. 3a, and for $p = 1/3$ in Fig. 3b. The behavior for $p = 1/3$ is representative of non-zero (positive) values of the allometric parameter. It is noteworthy that whatever Λ and p, all curves b_s cross the bifurcation point ($b = 0,\ \mu = 1$) where the bare soil solution b_0 changes stability. At this point, if $p = 0$, the slope $db_s/d\mu$ varies with Λ while it is independent from Λ if $p = 1/3$. In fact, for any $p > 0$, it is equal to -1, which is the slope of the (green) straight line $b_s = 1-\mu$ representing communities in which interactions are negligible ($\Lambda = 0$). Biologically, this makes sense because as b_s tends to zero, vegetation becomes sparsely distributed, mature plants are rare and, hence, interactions become negligible. Cooperativity then can have no effective influence. It is therefore intuitively clear that hysteresis, if it appears, would do so *via* a critical point whose coordinate b_c lies above the abscissa axis $b = 0$. In the 3-dimensional (b, Λ, μ)-space, the coordinates of this critical point are:

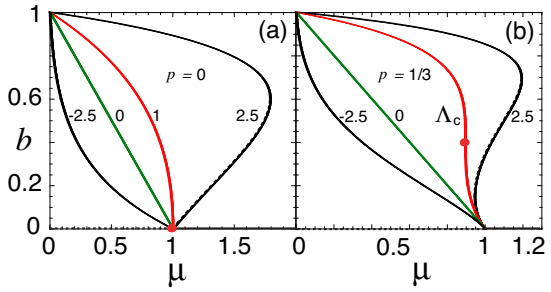

Fig. 3. Stationary states *vs* μ for different values of Λ. The red circle indicates the conditions for which hysteresis appears. (a) if $p = 0$, hysteresis appears at the point of intersection of the b_0 and b_s branches of solutions (*i.e.*, at zero biomass density); (b) if $p = 1/3$, it appears on the vegetated branch of solutions b_s at the critical point (16) *i.e.*, at a non-zero biomass density b_c. Dashed curves correspond to unstable states.

$$b_c = \frac{2p}{1+2p},\ (\Lambda^{-1})_c = b_c^{2p},\ \mu_c = \frac{e^{b_c}}{1+2\,p}. \tag{16}$$

Remarkably, the sole knowledge of the allometric parameter p suffices to evaluate these coordinates. For the field value $p = 1/3$, they are:

$$\begin{aligned} b_c &= \frac{2}{5},\ (\Lambda^{-1})_c = \left(\frac{2}{5}\right)^{\frac{2}{3}} \approx 0.543, \\ \mu_c &= \frac{3}{5}\exp(2/5) \approx 0.895. \end{aligned} \tag{17}$$

For $p = 0$, the slope of the curve b_s at its intersection with $b = 0$ (bare soil) is negative when $\Lambda < 1$, infinite for $\Lambda = 1$ and positive for $\Lambda > 1$. In other words, when $p = 0$, hysteresis appears on the abscissa axis under conditions where the biomass density is zero, where, as mentioned, interactions are nonexistent and where edaphic factors should not influence dynamics. One can only conclude from this that setting $p = 0$ is a crude approximation that should be avoided. This is certainly so in the modeling of vegetation at low biomass density and/or undergoing a desertification process.

3.2. *Stability diagrams*

Let $f_p\,[b(t)]$ be the expression between brackets on the right hand side of Eq. (13). The function

$$\mathcal{F}_{0,p}\,[b(t)] = -\int f_p\,[b(t)]\, db(t) \tag{18}$$

is a potential that completely determines the stability of the stationary states b_0 and b_s with respect to uniform perturbations that, in Fourier space, correspond to the mode $k = 0$. These states are the extrema of (18). They are linearly (locally) stable or unstable according to whether they are a minimum or maximum. The locus of stationary states where the second derivative of $\mathcal{F}_{0,p}$ changes sign is by definition called the *spinodal curve* (Korteweg, 1891). Its expression is given by Eq. (A.6) in appendix A. When, for given values of Λ^{-1} and μ, the potential $\mathcal{F}_{0,p}$ exhibits more than one minimum, the one that confers the smallest value to $\mathcal{F}_{0,p}$ is said to be stable (more precisely, *globally stable*). The others are called *metastable*. The locus of points where,

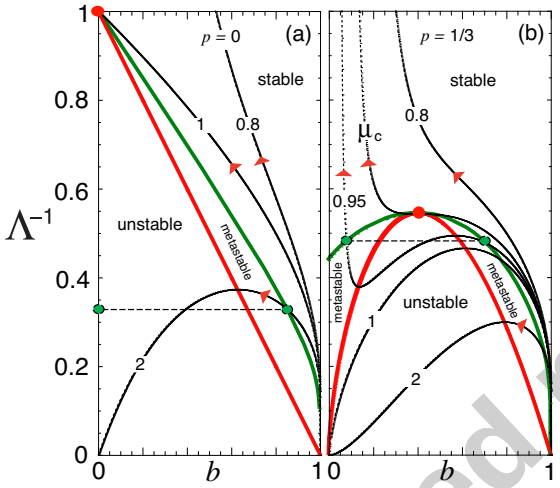

Fig. 4. Stability domains in (Λ^{-1}, b) space: in (a) for $p = 0$, in (b) for $p = 1/3$. The arrows indicate the direction of b_s's pathway of change when competition increases faster with aridity than facilitation.The red circle indicates the position of the critical point. The green circles joined by a dashed line represent two locally stable stationary states corresponding to the same values of μ and Λ (bistability), which are in equilibrium, *i.e.*, whose potential value $\mathcal{F}_{0,p}$ as given by (A.7) ($p = 0$) or by (A.8) ($p = 1/3$) is the same.

for given Λ^{-1} and μ, two locally stable stationary states are in equilibrium, *i.e.*, have equal values of $\mathcal{F}_{0,p}$, is by definition called the *connodal curve* (also often called the *binodal curve*). In the absence of a general analytical expression for it, the connodal curve can easily be calculated numerically (cf. green curves in Fig. 4).

The explicit expressions of the potential functions $\mathcal{F}_{0,p}$ for $p = 0$ and $p = 1/3$ are given in appendix A.2 (cf. (A.7), (A.8)). Fig. 4 reports the stability diagrams based on these expressions. The (Λ^{-1}, b)-space consists of three domains where b_s is globally stable (above the green connodal curve), metastable (between the red spinodal and green connodal curves) or unstable (in the spinodal domain situated under the red spinodal curve). Quantitatively, as well as qualitatively, Fig. 4a and Fig. 4b are very different. They further illustrate the shortcomings that arise when approximations completely erase the existence of a gradient of plant development: for $p = 1/3$, as for any $p \neq 0$, the spinodal curve crosses the abscissa at $b = 0$ and $b = 1$. In between, at the critical point (17), it passes through a maximum. In comparison, for $p = 0$, *i.e.*, when the influence of plant development is neglected, the spinodal abruptly becomes a straight line joining the points (0,1) and (1,0). As a result, the shape and size of the unstable, metastable and stable domains undergo a drastic singular transformation; simultaneously, the critical point (cf. red circle) becomes a transcritical saddle-node point of bifurcation situated on the ordinate axis at $\Lambda^{-1} = 1$. Given these pathologies, we focus in the following sections on the case $p \neq 0$, and more specifically on the case $p = 1/3$ relevant for Fig. 1.

3.3. *Influence of aridity on interactions and b_s pathway of change in (Λ^{-1}, b)-space*

All evidence indicates that climatic aridity due to water scarcity decreases the productivity of plant ecosystems. As most models assume, this decrease can be attributed, at least to some extent, to an increase of the loss/gain ratio μ. It is also known that water scarcity may give rise to pattern formation and ultimately, at unendurable levels of aridity, to vegetation death and desertification (Lefever and Lejeune, 1997; HilleRisLambers *et al.*, 2001; von Hardenberg *et al.*, 2001).

Before investigating the dynamics underlying these phenomena, it is useful to sort out vegetation kinetic responses to climatic variability and to examine the pathway of stationary curves b_s in (Λ^{-1}, b)-space. We therefore consider the combined effects of climate on the loss/gain ratio μ and on the feedback strengths χ_f, χ_c. Besides the fact that aridity increases μ, it also influences the synergies on which the functioning of ecosystems depends. It enhances or attenuates the interactions between neighboring plants. Shading and increased soil permeability that produce facilitation (embodied by χ_f) and competition for soil water resources (embodied by χ_c) have

different, probably weaker, effects in wet regions compared to arid regions. Furthermore, given that χ_f and χ_c correlate with different structures (crown and rhizosphere), functions (*e.g.*, shading and water uptake) and edaphic factors (Barbier *et al.*, 2008), it is likely that the variation of these parameters with aridity is different. This can result into significant variations in cooperativity $\Lambda = \chi_f - \chi_c$, or equivalently of Λ^{-1}. Increasing values of Λ^{-1} thus mean that competition increases more rapidly than facilitation.

Writing the stationary state equation (14) as

$$\Lambda^{-1} = \frac{b_s^{(1+2\,p)}}{\ln\left(\dfrac{\mu}{1-b_s}\right)}, \qquad (19)$$

the dotted curves calculated with (19) and plotted in Fig. 4 show how b_s evolve in the (Λ^{-1},b)-stability diagram for given μ. Considering these curves, one sees how the transition from uniform vegetation cover, to patterned organization and to desert may take place. Assuming that μ increases monotonously with the deficit of precipitation against potential evapotranspiration (referred to as "aridity") while Λ^{-1} behaves in a less regular manner, theoretical predictions in regard to increasing levels of climatic aridity can be schematized as follows:

Wet climate: The loss/gain ratio is small and allows for maximum biomass growth ($0 \lessapprox \mu \ll 1$). If water supply is abundant, competition for water is negligible ($\chi_c \approx 0$). Whether facilitation is large or small is a matter of secondary importance: the biomass distribution is uniform, its density is high ($b_s \approx 1$) and, most likely, corresponds to a system situated in the stable domain on a stationary state curve that remains in this domain, regardless of Λ^{-1} (cf. *e.g.*, the curve labeled 0.8 in Fig. 4b). The potential $\mathcal{F}_{0,1/3}$ has two extrema: the first one for $b = b_0$ is always a maximum and thus unstable, the second one is a minimum whose position evolves along the univalued stationary curve b_s.

Dry climate: The ratio of precipitation against potential evapotranspiration (humidity index) is sufficiently low to causes an increase of μ, which reaches values close to μ_c, but is still less than one. Facilitation is now more important because shading by crowns and/or organic material accumulation, which favors water infiltration and conservation, becomes a crucial element that compensates, at least partially, for the increases of μ and of χ_c. As a result, b_s belongs to a curve passing through or close to the critical point (16) (cf. *e.g.*, the curves labeled μ_c or 0.95 in Fig. 4b). Fig. 5 reports the behavior of the potential $\mathcal{F}_{0,1/3}$ for $\mu = 0.92$, *i.e.*, slightly above the critical value μ_c. The ecosystem exhibits a hysteresis loop when $0.485 \lessapprox \Lambda^{-1} \lessapprox 0.517$. Accordingly, $\mathcal{F}_{0,1/3}$ exhibits two minima. When $\Lambda^{-1} \approx 0.5097$, the values of $\mathcal{F}_{0,1/3}$ at these minima are equal (cf. the green circles joined by a horizontal, dotted tie line). In that case, the minima represent equilibrium states of quite different density. Facilitation stabilizes the highly vegetated state (cf. *e.g.*, the curve for $\Lambda^{-1} = 0.508$). Increased competition, on the contrary, makes it metastable (cf. *e.g.*, the curve for $\Lambda^{-1} = 0.513$) and ultimately suppresses it for $0.517 \lessapprox \Lambda^{-1}$. The low density state is then the only (globally stable) uniform solution possible. The bare soil state b_0 is always unstable and, hence, cannot be reached.

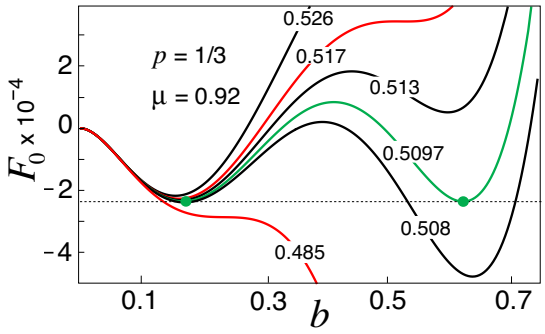

Fig. 5. Behavior of the potential function $\mathcal{F}_0$ under dry climatic conditions for the values of Λ^{-1} indicated.

Semiarid to arid climate: Potential evapotranspiration is now very large compared to rainfall and μ is greater than one. The vegetation is confronted with rising levels of competition χ_c. Facilitation is unable to compensate for this so that Λ^{-1} increases, which drives the community into the metastable and unstable spinodal domains following curves like those labeled 1 or 2 in Fig. 4b. Hysteresis becomes a more complex phenomenon since now it may also involve the bare soil state b_0, which may be metastable or stable.

4. Variational dynamics in dry climate, *i.e.*, for $\mu \approx \mu_c$ but inferior to 1

Variational behaviors are exceptional in spatially extended non-equilibrium systems. Up to now, they have only been reported in fields distant from ecology like hydrodynamics (Swift and Hohenberg, 1977; Pomeau and Manneville, 1980), chemistry

(see *e.g.*, Hilali *et al.*, 1996) or non-linear optics (see *e.g.*, Tlidi *et al.*, 1998). It is remarkable that such behavior can be demonstrated in the modeling of vegetation communities, at least, when they function in the vicinity of the critical point (16). This happens under the conditions classified as *dry climate* in section 3.3. The demonstration is given in appendix B. For the sake of the discussion below, we outline here its main idea and outcome.

The demonstration stems from the observation that at the critical point, by definition, the following two conditions are satisfied:

$$\omega_0 = 0 \quad \text{and} \quad \left(\frac{\partial \omega_k}{\partial k}\right)_{k=0} = 0. \tag{20}$$

The first condition states that the rate of regression of uniform perturbations, given by ω_0 and corresponding in Fourier space to the zero-mode ($k = 0$), is equal to zero. It expresses that the critical point is a state of marginal stability. This is easily verified by setting $k = 0$ and by replacing b_s and Λ with their critical values (16) in the eigenvalue equation (A.2) describing the time-evolution of Fourier modes. The second condition always holds for $k = 0$. Indeed, because the environment is isotropic, (A.2) can only depend on even powers of the modulus k, in fact on k^2. Thus, given (20), if

$$(\partial^2 \omega_k / \partial k^2)_{k=0} > 0,$$

then there exists a finite band of non-zero Fourier modes for which the uniform vegetation cover b_c, corresponding to the critical point, is unstable. This inequality is interesting. Before we carry on with the investigation of dry climate environments, it merits some general comments. Its explicit expression is of the form:

$$\varepsilon = \left(\frac{L_f}{L_c}\right)^2 < \left(\frac{\chi_c}{\chi_f}\right) \frac{1}{1 + \left(\frac{\delta}{\sigma}\right) F(b)}, \tag{21}$$

where $F(b)$ is a positive definite function and

$$d \equiv \delta / \sigma \tag{22}$$

is the vegetation transport (dispersion) coefficient. Inequality (21) shows that vegetation patterning is a phenomenon fundamentally due to plant-plant interactions. Vegetation propagation may suppress it, but it does not create it: pattern formation can only take place if the influence of interactions is not overwhelmed by the efficiency of vegetation propagation. If seed production (δ) and/or the dispersion range ($L_D = \sqrt{L_a/\sigma}$) increase while ε and χ_c/χ_f remain constant, then in the strong propagation limit, $d \to \infty$, inequality (21) reduces to the condition $\varepsilon < 0$. Clearly, it is then an unphysical condition that can never be satisfied. In fact, the most favorable conditions for patterning correspond to the weak propagation limit $d \to 0$. From a practical point of view, in regard to the system shown in Fig. 1, the field value $\varepsilon \approx 0.41$ is a given, measured constant. As such, it sets a lower bound below which the interaction ratio χ_c/χ_f may not decrease for a symmetry breaking instability to be possible.

In brief, inequality (21) supports the interpretation that vegetation patterns displaying characteristic lengths much larger than the size of individual plants originate from plant-plant interactions that affect biomass development through short range activation (L_f) and long range inhibition (L_c) effects (Lefever and Lejeune, 1997; Lejeune *et al.*, 1999). If the efficiency of seed production and/or propagation increases, this can only lead to the suppression of such large-scale structures and the restoration of a uniform vegetation cover.

Suppose now that the system is close to the critical point (16), that inequality (21) is satisfied and thus that there exists a finite band of unstable Fourier modes. Let k_f be the fastest growing mode of this band. Owing to the proximity of the critical point, k_f can be expanded in terms of a smallness parameter $0 < \eta \ll 1$ measuring the deviation from criticality. Furthermore, k_f evolves on a (slow) time scale $t^* \propto \eta^2$. Redefining the units of space and time by the transformation

$$\mathbf{r} \to \frac{\mathbf{r}}{k_f}, \quad t \to \frac{t}{\eta^2 t^*}, \tag{23}$$

one can then expand Eq. (1) in terms of η and show that the excess biomass density $\beta(\mathbf{r}, t)$, defined by the change of variable

$$b(\mathbf{r}, t) = b_c \left[1 + \eta \, \beta(\mathbf{r}, t)\right], \tag{24}$$

obeys to the fourth order partial differential equation (PDE) of Swift-Hohenberg form

$$\begin{aligned} \partial_t \beta(\mathbf{r}, t) = &- \mathrm{M} + \mathrm{K}\, \beta(\mathbf{r}, t) - \beta(\mathbf{r}, t)^3 \\ &+ \Gamma \left(\nabla^2 + \frac{1}{2} \nabla^4\right) \beta(\mathbf{r}, t). \end{aligned} \tag{25}$$

It is well-known that this type of Swift-Hohenberg equation describes a variational dynamics. Eq. (25) thus predicts that over the course of time, the community will strive to reach a stationary state, whether it is uniform or not, conferring the smallest possible value compatible with the imposed climatic constraints to the potential function $\mathcal{F}[\beta(\mathbf{r}, t)]$ given

by (A.9). $\mathcal{F}[\beta(\mathbf{r},t)]$ is therefore called the generator of the system evolution. It can be interpreted as a "spatio-temporal kinetic potential" that governs the global stability of the spatially extended non-equilibrium system considered; it is a generalization of the standard potential (18), which always exists for uniform systems and was used in section 3 to determine their global stability properties.

The dependence of the new loss/gain ratio M, cooperativity K and constant Γ upon the structural parameters p, ε and reproduction parameters δ, σ is given in appendix B. The essential property to keep in mind for the following is that the constant Γ, which as explained in section 4.2, plays both the role of a diffusion coefficient and of a line tension coefficient, *is always negative*.

An great advantage of the Swift-Hohenberg equation lies in the fact that it permits to obtain analytical expressions for the instability conditions of the density field that are easy to interpret. Notably, the dominant unstable mode k_f can be evaluated in terms of the structural parameters (L_a, p, ε), the interaction strengths (χ_f, χ_c), the kinetic parameter (μ) and the transport coefficient (δ/σ) (see Eq. (36) in section 4.3 and Eqs (B.11-B.15) in appendix B). These analytical expressions are studied and compared to field data in sections 4.1-4.3 below. They clarify the kinetic mechanism underlying vegetation patterns, its properties in relation to plant structure and exogenous factors, the similarities between self-organization in plant ecology and other domains.

4.1. *Local stability with respect to fluctuations in the PDE approximation*

We have shown in Fig. 4 that the stationary states b_0 and b_s are locally unstable with respect to uniform perturbations when these states fall into the spinodal domain of stability diagrams. Let us now study the local stability of uniform vegetated covers with respect to arbitrary, non-uniform fluctuations. Using (25), the treatment of this problem is quite straightforward. The coordinates of the critical point are now

$$\{\beta_{sc}, \mathrm{K}_c, \mathrm{M}_c\} = \{0, 0, 0\}. \tag{26}$$

Let β_s be a uniform stationary solution of (25). One easily finds that a Fourier mode k is stable or unstable depending upon whether its eigenvalue

$$\omega_k = \mathrm{K} - 3\,\beta_s^2 - \Gamma\,k^2\left(1 - \frac{k^2}{2}\right), \tag{27}$$

calculated with (25), is negative or positive. Given the rescaling of space (23), one sees that $k_f = \pm 1$. Putting $k = k_f$ in (27), one immediately obtains

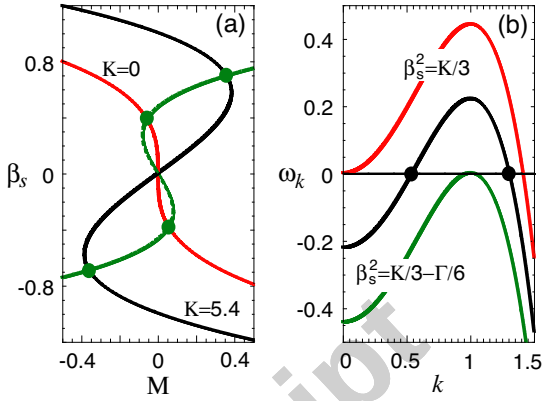

Fig. 6. (a) Excess stationary density β_s as a function of M for $\Gamma = -0.8849$, $\mathrm{K} = 0$ (in red: stationary curve when cooperativity equals its critical value) and $\mathrm{K} = 5.4$ (in black: a stationary curve displaying hysteresis). The intersections (green dots for $\beta_s = \beta_\pm$) with the green line are the bifurcation points of the symmetry-breaking instability. (b) Linear stability of the excess stationary densities β_s. The black curve displays a finite band of unstable modes; the black dots are its lower and upper cut-offs k_ℓ and k_u.

that for

$$\beta_+ \geq \beta_s \geq \beta_-, \tag{28}$$

where

$$\beta_\pm = \pm\sqrt{\frac{1}{3}(\mathrm{K} - \frac{\Gamma}{2})}, \tag{29}$$

there exists a band of unstable modes if

$$\mathrm{K} \geq \Gamma/2. \tag{30}$$

In Fig. 6a, the domain where uniform vegetation covers are unstable (cf. (28)) is the part of the stationary state curves β_s found between the green dots. One notes that such a domain already exists for the critical stationary state curve, *i.e.*, the curve for $\mathrm{K} = 0$, passing through the critical point. For $\mathrm{K} = 5.4$ (black curve), one notes that the instability occurs on part of the upper and lower branches of the hysteresis loop, which are stable with respect to uniform perturbations. The behavior of the band of unstable modes when β_s varies is represented in Fig. 6b. The lower and upper cut-offs of this band are, respectively, $k_\ell = k_-$ and $k_u = k_+$, where

$$k_\pm = 1 \pm \sqrt{1 - \frac{2}{\Gamma}\,(\mathrm{K} - 3\,\beta_s^2)}. \tag{31}$$

Remembering that Γ is negative, one notes that condition (30) may even hold for some negative values

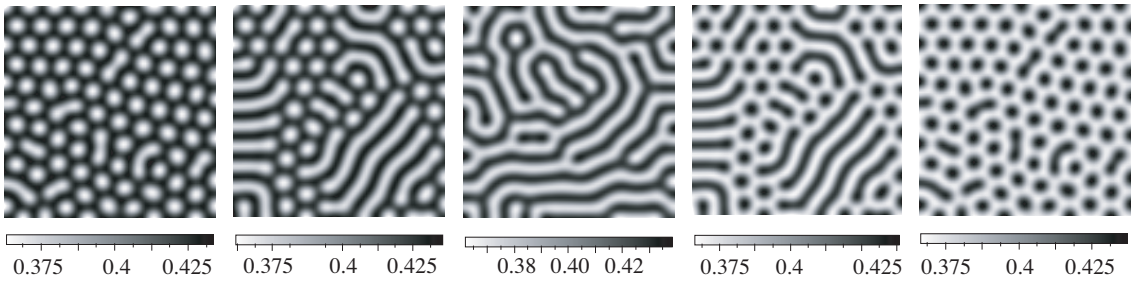

Fig. 7. Stationary patterns in the vicinity of the critical point for K = 0. Parameters have been determined so that the wavelength is approximately equal to 50 meters: $p = 1/3$, $\Gamma = -0.8849$, $\chi_f \approx 3.408$, $\varepsilon = 0.4096 \approx \chi_c/\chi_f$, $L_a \approx 1.080$ m and $\delta = 0$. The average initial conditions $\langle b(\mathbf{r},0)\rangle = b_c\,[1 + \eta\,\langle \beta(\mathbf{r},0)\rangle]$ indicated are calculated for $\eta = 0.1$ and $b_c = 2/5$.

of the (excess) cooperativity K. Thus, some modes may already be unstable before the cooperativity Λ is larger than its critical value (16). In that case, the uniform states that are unstable belong to stationary state curves situated outside of the spinodal domain (*i.e.*, above the red spinodal curve in Fig. 4b). In the following, we shall denote by k^* the non-zero fastest mode k_f when it satisfies the marginality conditions: *i.e.*, we shall set $k_f = k^*$ when

$$\omega_{k_f} = 0 \text{ and } \left(\frac{\partial \omega_k}{\partial k}\right)_{k=k_f} = 0. \qquad (32)$$

For the climatic conditions studied in this section, this happens when $\beta_s = \beta_\pm$ (cf. (29) and the green curve in Fig. 6b). The red curve in Fig. 6b corresponds to the saddle-node points of the hysteresis loop that exists when K > 0, or to the critical point if $K = K_{sc} = 0$ and $\beta_s = \beta_{sc} = 0$. The black curve in Fig. 6b is typical of systems undergoing an instability that could lead to pattern formation.

Fig. 7 shows examples of patterns predicted for fixed K = 0 and $\Gamma = -0.8849$. The snapshots are obtained by integrating (34) numerically with zero flux (Neumann) boundary conditions and the average initial densities $\langle b(\mathbf{r},0)\rangle$ indicated. The same noise (less than 1% of $\langle \beta(\mathbf{r},0)\rangle$ and zero mean value) has been added to all initial conditions. As β_s decreases (or equivalently, as the loss/gain ratio increases), the sequence of morphologies displayed by the patterns obtained is similar to that found by previous studies (cf. *e.g.*, Lefever and Lejeune (1997); von Hardenberg *et al.* (2001)): high, intermediate or low initial average biomass densities respectively evolve into a pattern formed of holes distributed throughout a uniform vegetation cover (gapped pattern), into more or less randomly oriented bands (labyrinthine tiger bush), or into a regular distribution of vegetation patches on bare soil (spotted patterns). We shall report on the situations arising when K > 0 elsewhere since this discussion would take us too far away from gapped patterns and desertification, which are our main subjects of interest here.

4.2. *Diffusional nature of the instability*

Eqs (25,A.9) demonstrate that the instability underlying vegetation patterns is a *diffusional instability*: it is caused by the negative "diffusion coefficient" Γ multiplying the laplacian term in (25). This unusual sign for a diffusion coefficient confirms, as pointed out in the discussion of (21), that vegetation patterning is fundamentally caused by plant-to-plant interactions and that vegetation propagation is a process of subordinate importance in this respect. Inspecting the explicit expression of Γ in terms of the system parameters (cf. (B.15), in which the constant Δ represents the biomass gains due to seeds), one notes that the limited influence of propagation does not take the simple, trivial form of dispersion terms to be negligible in comparison with those due to interactions. More subtly, dispersion manifests itself through the factor $(1-\Delta)^2$. Obviously, whatever the magnitude of Δ, this factor cannot change the sign of Γ and, in doing so, exert a control upon the origin of vegetation self-organization, *i.e.*, upon the existence of a negative diffusion coefficient. However, in agreement with our comments at the beginning of this section one sees that, through conditions (30) and (21), dispersion (Δ) may control the existence of a band of unstable modes. For example, with the field values $p \approx 1/3$ and $\varepsilon \approx 0.41$, (B.15) predicts that

$$\Gamma \approx -0.883\,(1-\Delta)^2,$$

and thus that there exists a band of unstable modes if $\Delta \approx 0$, $\mathrm{K} > -0.441$ and the competition strength χ_c is big enough for inequality (21) to be satisfied with $\varepsilon = 0.41$. If all other parameters stay constant while dispersion increases, this band is suppressed when $\Delta = 1$ at the latest, or possibly before that if inequality (21) no longer holds for $\varepsilon = 0.41$. On the other hand, for $\Delta > 1$, the expression of the marginal mode k^* becomes unphysical (see, (36) below), which, besides the violation of condition (21), is a further reason that the reappearance of a band of unstable modes for values $\Delta \gg 1$ becomes impossible. The situation $\Gamma = 0$ met when $\Delta = 1$ is not generic and cannot be studied in the framework of the Swift-Hohenberg PDE approximation; its discussion is therefore beyond the scope of this paper. To conclude our examination of Γ properties, it is worth commenting that the finding that Γ cannot change sign is fortunate. If Γ could could change sign, the status of the Swift-Hohenberg PDE (25), as a consistent approximation of (1) would be compromised. Indeed in (25), Γ is not only a diffusion coefficient but also the line-tension coefficient that multiplies the bilaplacian term. When Γ is negative this higher order derivative term is stabilizing, prevents the unbounded growth of unstable modes and, in this manner, insures the establishment of a stable pattern. This property would be lost if Γ could be positive and this loss would jeopardize the expansion procedure that permits to obtain (25).

Let us comment now on the similarities between the mechanism producing vegetation patterns and the better known mechanisms of phase separation in fluids. The following situation clarifies this aspect. Taking the critical point (26) as unperturbed state, one sets $\mathrm{M} = 0$, $\mathrm{K} = 0$ in Eqs (25,A.9) which become

$$\partial_t \beta(\mathbf{r},t) = -\beta(\mathbf{r},t)^3 + \Gamma\left(\nabla^2 + \frac{1}{2}\nabla^4\right)\beta(\mathbf{r},t) \tag{33}$$

and (A.10). Small deviations $u(\mathbf{r},t)$ from the critical density $\beta_{sc} = 0$ obey the linear continuity equation

$$\partial_t u(\mathbf{r},t) = \Gamma\left(\nabla^2 + \frac{1}{2}\nabla^4\right)u(\mathbf{r},t), \tag{34}$$

which gives the short-time dynamics of (33). Since Γ is negative, the diffusion process (34) takes on an unusual complexion. To see what is happening, one inspects its eigenvalues

$$\omega_k = -\Gamma\, k^2\,(1-k^2). \tag{35}$$

One notes that (35) is formally identical to the eigenvalue equation associated with generalized diffusion equations encountered in classical first order phase transition theory (see *e.g.*, Langer, 1991). It reflects the competition between clustering forces, which at the level of the factor $(1-k^2)$ favor phase separation (spinodal decomposition) at small k, and the diffusion limitation expressed by the factor k^2, which tends to slow this separation. The fastest mode $k_f = 1$, as a result, dominates in the system evolution. In fact, it grows exponentially and determines the wavelength of emerging patterns. However, as the snapshots in Fig. 7 show, in the case of vegetation, little coarsening takes place in the subsequent nonlinear regime: remarkably, in spite of the positive definite term $-\Gamma\left[\left(\nabla^2+1\right)\beta(\mathbf{r},t)\right]^2$, which represents in (A.10) the extra energy associated with departure from uniformity and which the variational property of the dynamics necessarily strives to minimize, the characteristic length of the stationary pattern finally obtained is in general still strongly dominated by the mode k_f.

In conclusion, on a short time scale dominated by diffusional instability, vegetation patterning evolves like a phase separation process in a binary mixture composed of bare soil and vegetation. On a long time scale, however, because the dynamics does not conserve the total number of particles (plants), the non-linear scalar term $-\beta(\mathbf{r},t)^3$ of (33) comes into play and prevents the complete separation into two "macroscopic phases", *i.e.*, two uniform regions, a vegetated region and a bare soil region separated by a minimal interfacial region.

4.3. *Comparison of predictions for dry climate with field data*

In physical units, at the dominant order of expansion (B.8), the wavelength of the marginal mode k^* reads:

$$\lambda = \frac{\pi L_a}{\sqrt{\eta}\left[\frac{8}{5}\left(\frac{1+4\,p}{1+6\,p}\right)(1-\varepsilon)(1-\Delta)\right]^{1/2}}. \tag{36}$$

In agreement with intuition, (B.12) shows that Δ is always positive. Furthermore, biomass gains due to seeds are generally negligible in comparison to those due to growth. The approximation $\Delta \approx 0$ should often apply; it certainly does for the system of Fig. 1. Hence, the wavelength λ only involves the plant structural parameters L_a, p, ε, which are directly accessible by field measurements, and the smallness parameter η, which, by definition for dry

climate, is smaller than 1. In fact, from the knowledge of these parameters, all critical properties can be predicted: we have already seen that the coordinates of the critical point (16) only depend on p; putting $\Lambda = \Lambda_c$ in (15) and $\chi_0 = \chi_c$ in (B.10) one obtains a very simple system of two equations,

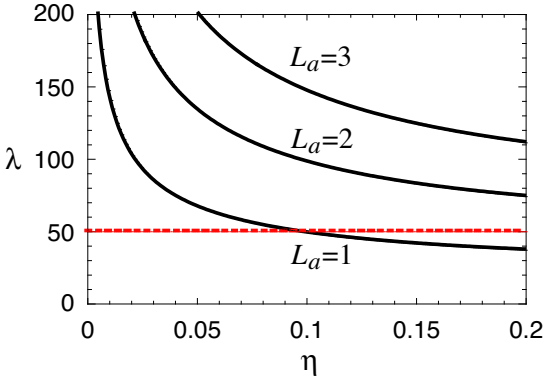

Fig. 8. Plot of the critical wavelength in meters predicted by Eq. (36) *vs* η for $p = 1/3$, K $= 0$, $\varepsilon = 0.4096$, $\delta = 0$ and the values of L_a indicated.

$$\Lambda_c = \chi_f - \chi_c, \quad \chi_c = \Lambda_c \left(\frac{\varepsilon}{1-\varepsilon} \right),$$

whose solutions χ_{fc} and χ_{cc} are the feedback values for which the marginal stability conditions (B.6) are satisfied at the critical point. For the field values $p \approx 1/3$ and $\varepsilon \approx 0.41$, this yields:

$$\chi_{fc} \approx 3.12, \quad \chi_{cc} \approx 1.28. \tag{37}$$

The behavior of the wavelength predicted by (36) for these values is shown in Fig. 8 as a function of η for three values of L_a:

$$\lambda \approx 3.66 \frac{L_a}{\sqrt{\eta}}. \tag{38}$$

When $\eta < 0.1$ and $L_a > 1$, the values obtained for λ are very large, in fact they are much larger than the 50 meters found in the field (represented by the red dashed line). Taking into account the histogram of Fig. 2, which indicates that the field values of L_a are close to 3 m, we conclude that for the system of Fig. 1, the predictions of the model are incompatible with the assumption of a system functioning close to the critical point (16).

5. Dynamics in arid climate for $\mu \geq 1$

Patterns displaying large variations between a densely vegetated state and bare soil as depicted in Fig. 1 only happen in arid climate where $\mu \geq 1$. Typically, such conditions correspond to large deviations from criticality that are not covered by the PDE approximation used in section 4. To study arid systems, one must go back to the full integro-differential version of the model, *i.e.*, Eq. (1). It is not possible through a linear stability analysis of this equation to obtain explicit expressions like (29,31). But fortunately, in practice, as shown in section 5.1, this difficulty can in many cases easily be bypassed thanks to the *a priori* knowledge of the pattern wavelength. When this essential information, accessible by field measurements, is known, calculation of explicit symmetry breaking conditions is straightforward. General results in this respect are established in section 5.1. They are used in the following sections to study the case $\mu \geq 1$ of particular interest here.

5.1. *Stability diagrams of non-zero modes*

To avoid cumbersome expressions, we set $p = 1/3$ and suppose that the approximation $\delta = 0$ is justified. The eigenvalue equation (A.2) then reads

$$\frac{\omega_k}{e^{\chi_f b_s^{\frac{5}{3}}}} = -b_s + \left[\chi_f\, \Omega_f(k) - \chi_c\, \Omega_c(k)\right](1-b_s)\, b_s^{\frac{5}{3}}. \tag{39}$$

The expressions of $\Omega_f(k)$ and $\Omega_c(k)$ are given in appendix A. For the following, one only needs to keep in mind that they are positive, which makes sense given the assumptions made in the modeling of the feedback functions $\mathcal{M}_f$ and $\mathcal{M}_c$. Inspection of (39) shows that b_s is always stable in the absence of facilitation. In order to determine instability conditions with respect to symmetry breaking fluctuations, one proceeds as in section 3.2: in the state space (Λ^{-1}, b), one determines the spinodal domain in which the mode

$$k^* \approx 2\,\pi\, \frac{L_a}{\lambda} \tag{40}$$

is unstable. In writing (40) one identifies λ (expressed in meters) with the wavelength of the fastest mode k_f satisfying the marginality conditions (32) and one supposes that this wavelength is given, approximately, by the wavelength measured in the field. This is often a good assumption. Replacing (40) in (32) yields a system of two equations, the solution of which

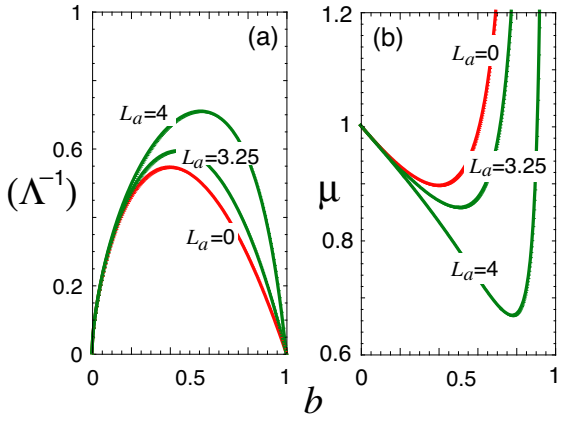

Fig. 9. (a) Spinodal curves in (Λ^{-1}, b)-phase space for $p = 1/3$, $\varepsilon = 0.4096$, $\lambda = 50$ m and the values of L_a indicated. Each curve divides the phase space into a domain (above the curve) where uniform biomass distributions are stable and a domain (under the curve) in which vegetation clustering can take place. (b) Spinodal curves in (μ, b)-phase space. The same values of parameters as in (a) are used. Above the curves, uniform biomass distributions are unstable.

$$\chi_f^* = -\frac{\Omega_c(k^*)'}{b_s^{2/3}\,(1-b_s)\,\Omega(k^*)}\,, \quad \text{where } ' \equiv \frac{\partial}{\partial k} \qquad (41)$$
$$\chi_c^* = \frac{\Omega_f(k^*)'}{b_s^{2/3}\,(1-b_s)\,\Omega(k^*)}$$

and

$$\Omega(k^*) = \Omega_f(k^*)\,\Omega_c(k^*)' - \Omega_f(k^*)'\,\Omega_c(k^*), \qquad (42)$$

gives the feedback levels χ_f^* and χ_c^* corresponding to marginal stability for the wavelength λ measured in the field. The expression of the spinodal curve of this wavelength in (Λ^{-1}, b)-space is then given by

$$(\Lambda^{-1})^* = 1/(\chi_f^* - \chi_c^*). \qquad (43)$$

It is represented in Fig. 9a for different values of the crown size L_a. The expression of the spinodal curve in (μ, b)-phase space is given by

$$\mu^* = (1-b_s)\exp\left(b_s^{5/3}\Lambda^*\right). \qquad (44)$$

It is represented in Fig. 9b. The spinodal domains in which vegetation patterns spontaneously form (under (above)the green curves in Fig. 9a (Fig. 9b)) always exceeds the spinodal domain of the mode $k = 0$ (under or above the red curve); these domains rapidly increase with L_a.

The coordinates of the critical point for the symmetry breaking mode k^*,

$$b = b_c^*,\ \Lambda_c^* = \Lambda^*(b_c^*),\ \mu_c^* = \mu^*(b_c^*), \qquad (45)$$

L_a	k^*	b_c^*	μ_c^*	$\chi_f^*(b_c^*)$	$\chi_c^*(b_c^*)$	Λ_c^*	$1/\Lambda_c^*$
0	0	0.400	0.895	3.12	1.28	1.84	0.543
3	0.377	0.470	0.871	4.14	2.39	1.75	0.573
3.25	0.408	0.507	0.856	4.49	2.78	1.71	0.584
4	0.503	0.780	0.667	10.2	8.53	1.68	0.596

Table 1
Symmetry breaking critical point values for $p = 1/3$, $\varepsilon = 0.4096$, $\lambda = 50$ m and the values of L_a indicated; $L_a = 0$ corresponds to the classical mean field idealization; $L_a \approx 3.25$ m corresponds to the largest crown size measured on the field for *Combretum micranthum*.

are obtained by replacing the solution, b_c^*, of the equation $\partial\mu^*/\partial b = 0$ in (43) and (44); μ^* is the smallest value of μ for which k^* becomes unstable. The critical coordinates (45) are reported in Table 1 for different values of the crown size. The case $L_a = 0$ corresponds to the mean field idealization (plants are points, densities refer to points and the wavelength of the critical mode is infinite (cf. (40)). Increasing L_a shifts b_c^* towards higher densities; simultaneously, the critical loss/gain ratio μ_c^* decreases, both χ_f^* and χ_c^* undergo a large increase, but without that the feedback difference Λ_c^* varies greatly.

In Fig. 10, the values of Table 1 for $L_a = 0$ and

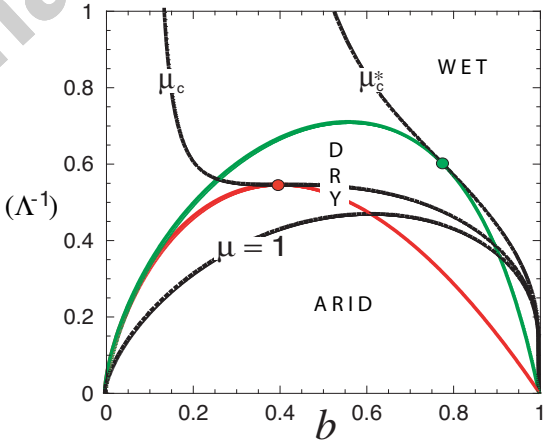

Fig. 10. Spinodal curves corresponding to $k^* = 0$ (mean field case, in red, $L_a = 0$) and $k^* = 0.503$ (symmetry breaking case, in green, $L_a = 4$ m, $\lambda = 50$ m, $\varepsilon = 0.4096$). The uniform stationary curves are plotted for $\mu^* = 0.667$, $\mu_c = 0.895$ and $\mu = 1$. The position of the mean field and symmetry breaking critical points are indicated by the red and green circles, respectively.

$L_a = 4$ have been used to represent the mean field (in red, $L_a = 0$) and symmetry breaking spinodal (in green, $L_a = 4$) together with the critical stationary

state curves tangent at their critical point and the stationary curve for $\mu = 1$. These curves divide the (Λ^{-1}, b)-space into three domains to which we shall refer as wet (above μ^*), dry (between $\mu = 1$ and μ^*, and containing μ_c) and arid (below $\mu = 1$) climate.

5.2. *Deeply gapped patterns*

In the case of deeply gapped patterns, the density switches periodically in space between a highly vegetated state and bare soil. Sufficient conditions for this to be possible are:
(i) Bare soil must be locally stable so that it can be reached in the course of the ecosystem evolution; this implies that the inequality $\mu \geqq 1$ holds.
(ii) Bare soil must be metastable with respect to some vegetated state b_s that is stable globally and situated beyond $\mu = 1$. Conditions (i-ii) are only met in arid climate allowing for the existence of a large hysteresis loop such as shown in Fig. 11. Furthermore, we show below that for b_0 to be metastable with respect to the vegetated state b_s, the crown L_a must be larger than some lower bound $\widehat{L_a}$.
(iii) The upper states of the hysteresis must exhibit a symmetry breaking instability whose bifurcation point is at $\mu \geqq 1$.
Hence, $\mu = 1$ is the smallest loss/gain ratio at which deep gapped patterns may appear when competition χ_c increases. For this to happen, the symmetry breaking instability must appear in its vicinity. Table 2 reports for increasing values of L_a the values of the other parameters calculated in imposing the condition that $\mu = 1$ is the bifurcation point of the symmetry breaking instability. This insures that conditions (i) and (iii) above are satisfied.
Condition (ii) requiring b_0 to be metastable with respect to the vegetated state b_s corresponding to $\mu = 1$ is more difficult to satisfy. For the theory presented, it constitutes a real test of its predictive value and capacity to quantitatively interpret the field data corresponding to the pattern shown in Fig. 1. There is indeed no free adjustable parameter left. The test thus consists of determining whether or not condition (ii) can be satisfied when one combines the results of Table 2 with the data of the histogram in Fig. 2. To investigate this question, one has to compare the value $\mathcal{F}_0(b_0)$ of the potential function (A.8) for bare soil with its value $\mathcal{F}_0(b^*)$ for the vegetated state b^* and the parameters calculated in Table 2. One easily finds that

$$\mathcal{F}_0(b_0) = 0, \quad \forall \mu \quad \text{and} \quad \forall L_a.$$

In Fig. 12, on the other hand, the behavior of $\mathcal{F}_0(b^*)$ as a function of L_a is plotted for the three values of μ indicated. Let $\widehat{L_a}$ be the value of L_a such that $\mathcal{F}_0(b^*) = 0$. Accordingly, b^* is stable and b_0 is metastable if

$$L_a > \widehat{L_a}. \tag{46}$$

One notes that for $\mu = 1$ and $1 \leq L_a \leq 3.173$, bare soil is stable and, thus, that the vegetated state b^* at which the symmetry breaking instability sets in is metastable. On the contrary, for $L_a > 3.173$, b^* is stable and bare soil is metastable. Table 3 gives the values of $\widehat{L_a}$ and the parameters at which $\mathcal{F}_0(b^*)$

L_a (m)	b^*	$\chi_f^*(b^*)$	$\chi_c^*(b^*)$	Λ^*	$1/\Lambda^*$
1	0.6130	3.774	1.628	2.146	0.4660
1.5	0.6160	3.967	1.821	2.146	0.4659
2	0.6246	4.284	2.137	2.147	0.4658
2.75	0.6610	5.225	3.068	2.157	0.4637
3	0.6848	5.817	3.647	2.170	0.4608
3.173	0.7068	6.408	4.220	2.188	0.4571
3.5	0.7654	8.405	6.141	2.264	0.4417

Table 2
Influence of L_a on marginality conditions (41,42) for $p = 1/3$, $\varepsilon = 0.4096$, λ=50 m and other parameters determined so that the symmetry breaking instability appears at $\mu = 1$.

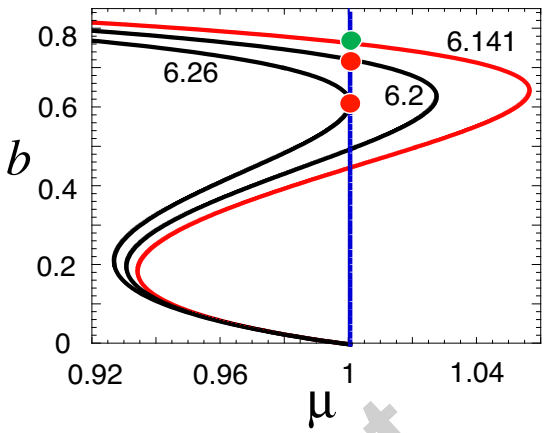

Fig. 11. Stationary curves b_s for $p = 1/3$, $\varepsilon = 0.4096$, $L_a = 3.5$ m, $\chi_f = 8.405$ (cf. Table 2) and χ_c as indicated. For $\chi_c = 6.141$ (red curve), the symmetry breaking instability appears at $\mu = 1$ (green circle) with $\lambda \approx 50$ m. For $\chi_c = 6.15$, the ecosystem develops a deeply gapped pattern. At higher levels of competition (red circles at $\chi_c = 6.20$ and 6.26), the organization transforms into bare bands and spots inside a uniform cover, and into vegetated bands and spots on bare soil (see Fig. 13).

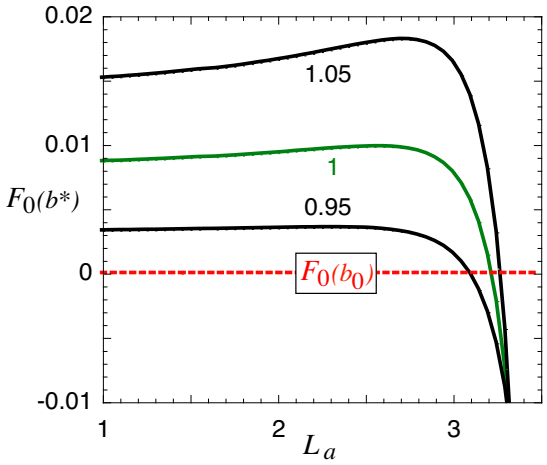

Fig. 12. Potential $\mathcal{F}_0(b^*)$ *vs* L_a for $p = 1/3$, $\varepsilon = 0.4096$, $\lambda = 50$ m and μ as indicated. For $\mu = 1$, $\mathcal{F}_0(b^*) = 0$ when $L_a = \widehat{L_a} \approx 3.173$.

μ	$\widehat{L_a}$ (m)	b^*	$\chi_f^*(b^*)$	$\chi_c^*(b^*)$	Λ^*	$1/\Lambda^*$
1	3.173	0.7068	6.408	4.220	2.188	0.4571
1.5	3.302	0.8194	10.11	7.163	2.950	0.3389
2	3.304	0.8491	11.95	8.551	3.394	0.2946
2.5	3.300	0.8648	13.23	9.509	3.716	0.2691
3	3.296	0.8749	14.22	10.25	3.960	0.2519
3.5	3.293	0.8821	15.03	10.85	4.179	0.2393

Table 3
Minimal size $\widehat{L_a}$ the crown of mature plants should exceed to satisfy condition (ii) *vs* μ for $p = 1/3$, $\varepsilon = 0.4096$, $\lambda = 50$ m.

changes sign for values of μ corresponding to arid climate. One sees that a variation of μ over a large interval from 1 up to 3.5 has little effect on the value of $\widehat{L_a}$, which remains approximately equal to 3.3 m. These results show that the allometric and structural parameters p, ε and L_a not only control the characteristics of vegetation patterns such as the distance between vegetated bands or patches, but also, through inequality (46), they control the very existence of the pattern itself. The other morphological parameters p and ε being given, $\widehat{L_a}$ can be viewed as a bench mark dividing plant species into two categories according to whether or not the crown L_a of their mature individuals is larger or smaller than $\widehat{L_a}$. In the first case, the upper state b_s of the hysteresis is more stable than bare soil. Therefore, the instability, when it appears, cannot trigger desertification but instead induces the formation of deeply gapped patterns. On the contrary, when L_a is somewhat smaller than $\widehat{L_a}$, desertification occurs abruptly, as soon as the stationary curve (19) reaches the symmetry-breaking spinodal (43).

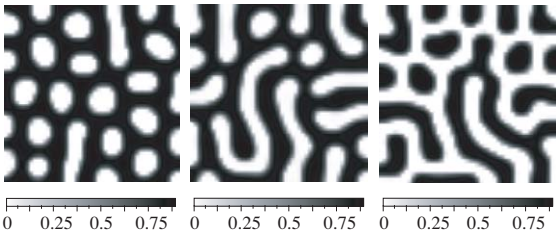

$\chi_c = 6.15$ $\chi_c = 6.200$ $\chi_c = 6.259$

$< b >= 0.5481$ $< b >= 0.5086$ $< b >= 0.440$

Fig. 13. Stationary patterns for the conditions depicted in Fig. 11 (green and red circles), *i.e.*, $L_a = 3.5$ m, $\chi_f = 8.405$ and increasing competition levels.

With regard to the question raised earlier concerning the predictive merits of the present theory, the discussion of Fig 12, and of the results of Tables 2 and 3 is satisfying. We find that the field data of Barbier *et al.* (2008), which fix the maximal crown size of mature plants at $L_a \approx 3.25$ m (cf. Fig. 2), validate the prediction reached here that, in order to exhibit deep gapped patterns, the maximal L_a for mature *Combretum micranthum* plants should exceed ≈ 3.17 m. A more complete investigation of the case $L_a < \widehat{L_a}$ is planned.

Fig. 13 shows the stationary patterns obtained by numerical simulation of Eq. (1) for $\mu = 1$, $L_a = 3.5$ and the green and red circles in Fig. 11 as initial conditions. For $\chi_c = 6.15$ (slightly inside the spinodal domain of the symmetry-breaking mode), as expected, the system evolves towards a deep gapped pattern: the vegetation cover exhibits a more or less regular distribution of bare soil spots. When competition increases, for $\chi_c = 6.2$, neighboring spots start to coalesce, giving rise to a labyrinthine morphology. Simultaneously, the average pattern density decreases while the maximal density of vegetated domains stays approximately constant, or slightly increases. At the saddle-node point ($\chi_c = 6.26$) a stable pattern still forms, indicating that this structured branch extends further, *i.e.*, to competition levels for which uniform solutions b_s do not exist: bare soil is then the only uniform solution possible. Under those conditions, development of a labyrinthine pattern of bands or spots distributed over bare soil (not shown) constitutes an adaptive behavior through which a significant

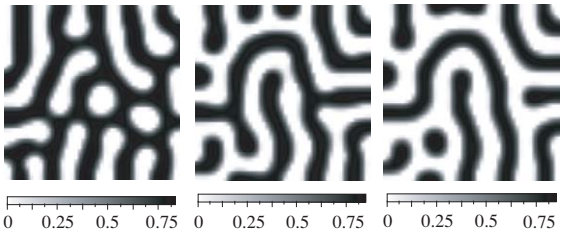

Fig. 14. Stationary patterns obtained for the value $L_a = 3.173$ m, at which b_0 and b_s exchange stability and metastability, for $\chi_f = 6.408$ and increasing competition levels χ_c.

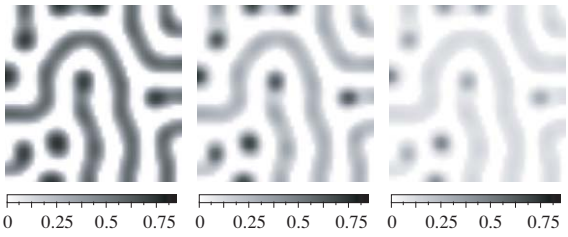

Fig. 15. Desertification: transition from stable pattern to bare soil when $L_a = \widehat{L_a} = 3.173$ m and Λ^{-1} significantly exceeds the saddle-node value of the mean field spinodal. The sequence of snapshots is taken after increasing the competition level from $\chi_c = 0.43$ to $\chi_c = 0.45$. The level of facilitation $\chi_f = 6.408$ is constant (see initial condition in Fig. 14).

average biomass density can still be maintained and extinction can be avoided.

Fig. 14 shows stationary patterns obtained for $L_a = \widehat{L_a} = 3.173$ m, which is the value at which the exchange of stability and metastability between bare soil and b_s takes place. For $\chi_c = 4.230$, conditions correspond to the neighborhood of the symmetry-breaking spinodal curve while for $\chi_c = 4.261$, they corresponds to the saddle-node point of the mean-field spinodal. When $\chi_c = 0.43$, though this value exceeds the hysteresis domain, a stable (subcritical) pattern still exists that exhibits essentially the same morphology as it does for $\chi_c = 4.261$, but with a lower average biomass.

5.3. *Two mechanisms of desertification: local desertification or gap coarsening*

Fig.15 illustrates the process of desertification from which the ecosystem can no longer escape if χ_c increases somewhat further. Taking the third pattern shown in Fig. 14 as the initial condition and setting $\chi_c = 4.5$, one sees a rapid decrease over time of the biomass density of the vegetated bands, as well as of the pattern's average biomass. One also notes that the evolution of vegetation towards extinction takes place more or less uniformly. It is a local process of desertification during which the biomass density decreases inside vegetated areas but without much effect on the morphological distribution of vegetated and bare soil areas.

In contrast, desertification may take place much more abruptly when the maximum crown size L_a is smaller than the threshold value $\widehat{L_a}$ at which $\mathcal{F}_0$ changes sign (The difference $\widehat{L_a} - L_a$ needs to be slightly positive). Fig. 16 illustrates this second mechanism. Considering that the loss/gain ratio has the value $\mu = 1$ as in Fig. 14 and 15, we suppose that the crown size L_a is equal to 2.75 m, *i.e.*, approximately 13% below the threshold value $\widehat{L_a} = 3.173$. As a result, the highly vegetated states b_s of the hysteresis are now metastable with respect to bare soil. The sequence of snapshots reported in the figure shows the evolution of an initial condition chosen very close (relative distance: $\approx 0.073\%$) to the bifurcation point at which the symmetry-breaking instability appears. The gapped pattern organization that appears on a short time scale is now a transitory regime. It is followed by a coarsening process that corresponds to the expansion of bare soil domains that coalesce and invade the entire territory. In the course of this evolution, the pattern progressively undergoes profound morphological modifications. In contrast to what happens in the case of Fig. 15 where vegetation bands tend to disappear by "local desertification", here the area occupied by vegetated bands in the territory progressively decreases but their biomass density stays approximately constant during most of the evolution (it may even increase at some spots); only when the biomass distribution is reduced to a small finite number of isolated spots does the maximum vegetation density finally decrease and rapidly tend to zero everywhere. The numerical integrations carried out suggest that coarse graining desertification starts as soon as the bifurcation point of the symmetry-breaking instability is crossed.

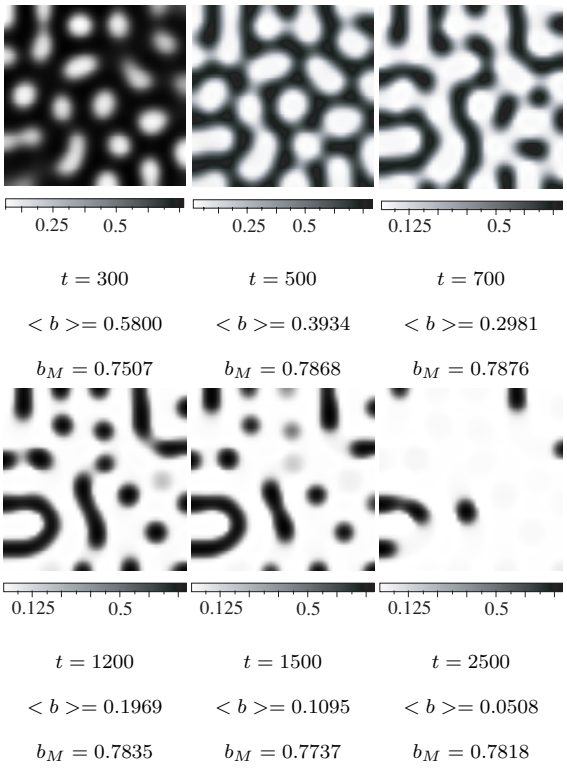

Fig. 16. Metastability of uniform vegetation cover: snapshots at different times showing the formation of a gapped patterns triggered by the symmetry-breaking instability and the subsequent transformation of this pattern *via* the gap coarsening process into uniform bare soil (desert) state. Values of parameters: $p = 1/3$, $\varepsilon = 0.4096$, $L_a = 2.75$ m, $\lambda = 50$ m, $\mu = 1$, $\chi_f = 5.224$, $\chi_c = 3.070$

6. Discussion

To capture the self-organization mechanisms of vegetation under isotropic environmental conditions, two kinds of approach have been developed in the literature. They differ in that they focus either on the vegetation patch level and the processes of water transport by above-ground run off and below-ground diffusion (HilleRisLambers *et al.*, 2001; von Hardenberg *et al.*, 2001) or on the individual plant level and the properties differentiating above- and below-ground plant structures as mediators of facilitation and competition (Lefever and Lejeune, 1997).

It is established (Barbier, 2006; Barbier *et al.*, 2008) that the hypotheses made within the framework of approaches dealing with water redistribution mechanisms do not apply to the site shown in Fig. 1. This site is representative in terms of constitutive species, soil substratum, pattern characteristics and climatic conditions of the vegetation patterns of South West Niger and was therefore used as a reference system in this paper. Gapped patterns with large standing vegetation have also been studied in Burkina Faso (Couteron and Lejeune, 2001). On the other hand, in the case of the second kind of approach which emphasizes the characteristics of plant structures, the original modeling, proposed more than ten years ago, needs an upgrade in order to account for the more recent field observations. The appropriate revisions made here are summarized as follows:

(i) In accordance with field results, facilitation and competition are now decoupled structurally and functionally in the modeling. These opposed forms of feedback operate independently and are mediated by plant's clearly separated above-ground and below-ground structures. Functionally, these feedback mechanisms contribute to opposed scale pans of the balance weighting biomass gains against biomass losses. Consistent with this fact, facilitation and competition have been remodeled through the feedback functions $\mathcal{M}_f$ and $\mathcal{M}_c$, and have been associated in Eq. (1) with the growth and loss terms respectively. It is noteworthy that since the approach is set up in terms of the characteristics of individual plants and not of vegetation patches, the biomass density $b(\mathbf{r}, t)$ refers to the surface element S occupied by a mature plant. This introduces the structural length L_a into the description, which is then shown to be a determining parameter controlling the stability of the vegetation cover. In this modeling procedure, the notion of feedback is spatialized; it strictly refers to interactions between plants. Processes through which a plant sustains its own biomass evolution, *e.g.*, the development of its own crown or of its own rhizosphere, do not qualify as feedback effects: self-facilitation or self-competition effects do not make sense here and are not postulated.

(ii) In order to take into account the influence of plant development on the range over which feedback operates, the educated guess (ansatz) consisting to let the facilitation and competition ranges L_f and L_c depend upon the biomass density has been introduced. From the modeling point of view, this has the advantage that it avoids the complication of increasing the number of variables that the consideration of several classes of age would otherwise impose. From a quantitative point of view, this guess can straightforwardly be calibrated to

fit the specificity of a particular plant by using the measured values of the allometric parameter p and structural ratio ε. So far, field values for these parameters are only known in the case of the reference site of Fig. 1. Hence, for the purposes of quantitatively illustrating our modeling predictions and of comparing their outcome with a concrete, well defined system, we have used the values $p = 1/3$ and $\varepsilon \approx 0.41$ corresponding to the shrub species *Combretum micranthum* G. Don, which predominates at this site. Whether similar values apply to other species is an open, fundamental and motivating question. It is hoped that the approach we report will stimulate further field work yielding progress and clarifications in this respect.

(iii) In the original modeling, both processes of biomass growth and biomass propagation (by seeds or vegetative) are lumped together in the gain term. Hence, the denomination of the *propagator-inhibitor model* as it has been called (Lejeune *et al.*, 1999; Couteron and Lejeune, 2001). These processes are now modeled separately. To describe propagation an integro-differential representation more appropriate and general than the usual laplacian approximation has been introduced. This has allowed us to qualitatively as well as quantitatively assess the influence of vegetation propagation on pattern formation. With regard to the pattern of reference, we conclude that there is no reason to interpret seed dispersal as a cause of deeply gapped pattern organization. Furthermore, the results clearly establish that when the range of seed dispersion L_D increases beyond some limit, pattern formation becomes impossible. Intuitively, one expects this prediction to be general, at least within the framework of a time continuous and space continuous approach like the one we adopted. It is however interesting to note that approaches describing biological invasions by processes that are discrete in time and discrete in space (cellular automata) predict the occurrence of fractal fronts when propagation is governed by long range power laws (see *e.g.*, Cannas *et al.*, 2006). We shall not venture here into the dangerous territory of comparing continuous and discrete modeling approaches. This is a difficult, non-trivial mathematical problem that is not our subject and lies beyond our biological objectives.

On the practical, empirical side, testable expressions have been obtained predicting the conditions of appearance of patterns and their characteristics in terms of a restricted set of parameters. This set is summarized as follows: (i) three structural parameters, L_a, p, ε, can be determined with precision by measurements carried out on the individual plants found in the field; (ii) two kinetic parameters, μ, δ/σ (the effective dispersion coefficient), describing biomass growth and propagation can be estimated for some species on the basis of existing literature; (iii) two feedback parameters, χ_f, χ_c, describe the strength of interactions between plants and the influence of edaphic or climatic factors on these interactions. The instability and desertification conditions of χ_f and χ_c are predicted by the theory (cf. expressions (41) and Tables 1-3). Using the data established by direct field measurements of the pattern wavelength and plant structural parameters, these expressions have permitted an in depth analysis of the ecosystem shown in Fig. 1.

A striking outcome of this analysis concerns the structural requisite regarding crown size, $L_a > \widehat{L_a}$, which insures that stable, deeply gapped patterns (that is bare patches within a vegetation matrix of rather high biomass density) can form under the arid climatic conditions as defined in section 3.3 and studied in section 5.2. This result demonstrates remarkable agreement between theoretical predictions and field observations. Given the measured field values $p = 1/3$ and $\varepsilon \approx 0.41$, the calculated value of $\widehat{L_a}$ for $\mu = 1$ (the smallest value of μ for which deeply gapped patterns are possible) is $\widehat{L_a} = 3.173$. On the other hand, independently from this theoretical calculation, field measurements yield $L_a \approx 3.25$ (cf. Fig. 2). Comparing these two values shows that the above inequality is satisfied for the ecosystem of Fig. 1. In other words, the theory predicts that deeply gapped patterns are indeed the organization that one should expect in the case of this system. One also sees in Table 3 that for $\mu > 1$, the values of $\widehat{L_a}$ rapidly increase with μ and thus become rapidly much greater than the field value of L_a estimated from Fig. 2. Considering that the reference pattern is a stationary, stable organization as multi-temporal remote sensing data indicate (Barbier *et al.*, 2006), this suggests that in reality this ecosystem functions under loss/gain conditions corresponding to μ close (superior or equal) to one.

Another original outcome of the modeling, which the simulations in Figs. 15 and 16 illustrate, is the prediction that vegetation extinction (desertification) can take place following the *gap coarsening pathway* which so far had not yet been described. Strikingly, this mechanism of extinction is met for smaller values of the loss/gain ratio μ than the *lo-*

cal desertification pathway, which takes place when the loss/gain ratio exceeds the (upper) turning point of the hysteresis loop. So far, it is this kind of situation that has been predicted as potentially catastrophic because it implies an abrupt transition of the ecosystem from a vegetated state (typically a more or less periodic distribution of vegetated spots) towards the bare soil state (von Hardenberg *et al.*, 2001; Rietkerk *et al.*, 2004). An even more catastrophic alternative is put into evidence here, namely, that the symmetry-breaking instability may trigger a transition that short-cuts the pattern organization stage. This causes the ecosystem to switch abruptly, without stable pattern formation, from a uniform, highly vegetated cover directly to the bare soil (desert) state. This mechanism is likely to take place much sooner, *i.e.*, well before the saddle-node point of the hysteresis is reached. It is the fate which, as aridity increases, awaits those species whose crown size L_a is significantly below $\widehat{L_a}$.

On the conceptual side, the prediction that the organization of vegetation communities is ruled by a critical point is all the more remarkable since the coordinates (16) of this point in $\{b, \Lambda, \mu\}$-space depend on the sole knowledge of the allometric parameter [1]. This prediction clarifies the nature of the instability underlying vegetation patterns. It also remedies a shortcoming displayed by all earlier self-organization models of vegetation patterns. To conclude, let us comment on these two aspects.

First, we note that (16) is a true ecological analogue of the physico-chemical conditions that govern the onset of immiscibility in regular solutions where unmixing is associated with the minimization of the energy rather than with the maximization of the entropy in the free energy. Self-organized landscape patterning obeys a mechanism that, phenomenologically speaking, has much in common with a phase transition in which vegetation and bare soil "phase separate" *e.g.*, like some polymer mixtures (Leibler, 1980; Bates, 1985) that display $3d$-organizations whose morphology in 2-dimensions recalls those of $2d$-vegetation patterns. Given the fact that close to the critical point vegetation patterning dynamics can be captured by a variational principle, generating a Swift-Hohenberg equation whose "diffusion coefficient" Γ is negative is the demonstration of this phase transition type of phenomenology. Seed dispersion is not a basic factor in this respect. Vegetation self-organizations originate from a diffusional instability due to interactions between plants. It would be appropriate to classify these organizations as such, rather than as the result of a Turing type of instability. The latter instability is a "chemical" phenomenon in the description of which interactions other than chemical reactions, *e.g.*, physical forces like the Van der Waals intermolecular interactions, play no role and can in general be completely neglected. A similar non-Turing interpretation also applies to the non-periodic (so called *glassy*) vegetation patterns of frozen disordered plant spots found in some arid regions (Shnerb *al.*, 2003; Maruvka and Shnerb, 2006).

From a theoretical modeling point of view, the introduction of the allometric parameter p not only crucially influences the order-disorder transitions involved in patterning and desertification, it also improves a weak point of previous self-organization models. In general, they either do not take into account the variation of interaction range with plant development, or they underestimate its influence (Lefever and Lejeune, 1997; HilleRisLambers *et al.*, 2001; von Hardenberg *et al.*, 2001; Zeng *al.*, 2004; Kéfi *et al.*, 2007). As Fig. 4 illustrates, setting $p = 0$ is a convenient approximation but quite unrealistic because it suggests that hysteresis, a phenomenon that requires large feedback effects, remains possible even when the biomass tends to zero, *i.e.*, under conditions where plants are so sparsely distributed that they cannot interact. This problem is automatically avoided when the allometric constant p is different from zero (positive) and by the modeling of $\mathcal{M}_f$ and $\mathcal{M}_c$, which insures that these functions tend to one (cf. (3)) when the biomass density tends to zero. Biologically speaking, our approach provides a reliable quantitative description of phytosocietal interactions for ground-limiting resources in terms of plant size and development at low and high biomass densities. It highlights the importance of the crown/root ratio, which reflects the plasticity of plant structures in the face of water stress and demonstrates that vegetation patterning is conceptually an order-disorder transition whose dynamics has properties similar to those of some phase separation processes.

[1] It is also interesting to note that species for which the inequality $p \gg 1$ would hold, reach criticality and thus patterning conditions for average biomass densities very close to one.

Appendix A. Stability of uniform states

A.1. *Linear stability of uniform stationary states*

Let

$$\delta b(\mathbf{r},t) = \frac{1}{2\pi}\int d\mathbf{k}\, A(\mathbf{k},0)\exp\left(\omega_k t + i\mathbf{k}\cdot\mathbf{r}\right) \quad \text{(A.1)}$$

be the decomposition into Fourier modes of an arbitrary infinitesimal fluctuation perturbing a uniform stationary state solution b of Eq. (1); $A(\mathbf{k},0)$ is the initial amplitude of the wave vector of modulus $k \equiv |\mathbf{k}|$. We replace $b(\mathbf{r},t) = b + \delta b(\mathbf{r},t)$, (2), (4-6) and (A.1) in Eq. (1), only retain the terms linear in $A(\mathbf{k},0)$. Hence, we obtain that the Fourier mode k is unstable if its eigenvalue

$$\begin{aligned}\omega_k = &\left[1-2b+\chi_f\Omega_f(k)(1-b)b^{(1+2p)}\right]e^{\chi_f b^{(1+2p)}} - \\ &\mu\left[1+\chi_c\Omega_c(k)\,b^{(1+2p)}\right]e^{\chi_c b^{(1+2p)}} - \\ &\delta\left(1-e^{-\frac{k^2}{4\sigma}}\right)\end{aligned} \quad \text{(A.2)}$$

is positive. Inspection of (A.2) and of the expressions

$$\begin{aligned}\Omega_f(k) =& \frac{(1+2p)}{(1+k^2b^{2p})^{\frac{5}{2}}}\left[1+\frac{k^2(1-p)}{1+2p}b^{2p}\right], \\ \Omega_c(k) =& \frac{(1+2p)\varepsilon^{\frac{3}{2}}}{(\varepsilon+k^2b^{2\,p})^{\frac{5}{2}}}\left[\varepsilon+\frac{k^2(1-p)}{1+2p}b^{2p}\right],\end{aligned} \quad \text{(A.3)}$$

shows that:
(i) For $p < 1$, both $\Omega_f(k)$ and $\Omega_c(k)$ are positive whatever the biomass density b or the structural ratio ε may be. It is interesting to note that facilitation rather than competition is likely to destabilize uniform states.
(ii) The third term of ω_k, contributed by plant propagation, is negative and thus always stabilizing. Furthermore, close to the critical point, this term is negligible for Fourier modes whose wave number is close to zero.
(iii) For $k \to \infty, \omega_\infty < 0$. Hence, the Fourier modes $k \gg 1$ are always stable. This is consistent with the requirement that the biomass distribution of the surface element S with respect to which the density $b(\mathbf{r},t)$ is defined must be uniform.
(iv) For bare soil, the eigenvalue ω_0 is simply:

$$\omega_0 = 1-\mu. \quad \text{(A.4)}$$

Thus, b_0 is linearly unstable with respect to uniform perturbations for $0 \le \mu < 1$ and linearly stable otherwise. On the other hand, using (14) to eliminate μ in (A.2) shows that for vegetated states

$$\omega_0 = b_s\left[-1+\Lambda(1+2\,p)\,(1-b_s)\,b_s^{2\,p}\right]e^{\chi_f\, b_s^{(1+2\,p)}}. \quad \text{(A.5)}$$

Accordingly, the spinodal curve (see Fig. 4)

$$\Lambda^{-1} = (1+2\,p)\,(1-b_s)\,b_s^{2\,p} \quad \text{(A.6)}$$

separates the (Λ^{-1}, b)-space into two domains where vegetated states are either stable (above the spinodal) or unstable (below the spinodal).

A.2. *Potential functions*

The potentials governing the global stability of uniform states when $p = 0$ and $p = 1/3$ read:

$$\begin{aligned}\mathcal{F}_{0,0}\left[b(t)\right] = &-\frac{b(t)^2}{2}+\frac{b(t)^3}{3}+ \\ &\frac{\mu}{\Lambda}e^{-\Lambda\, b(t)}\left[b(t)-\frac{1}{\Lambda}\right],\end{aligned} \quad \text{(A.7)}$$

$$\begin{aligned}\mathcal{F}_{0,\frac{1}{3}}\left[b(t)\right] = &-\frac{b(t)^2}{2}+\frac{b(t)^3}{3}+ \\ &\frac{\mu}{2}\frac{b(t)^{\frac{1}{6}}\,e^{-\frac{\Lambda}{2}\,b(t)^{\frac{5}{3}}}W_M\left(\frac{1}{10},\frac{3}{5},\Lambda\,b(t)^{\frac{5}{3}}\right)}{\Lambda^{10/11}}.\end{aligned} \quad \text{(A.8)}$$

$W_M\left(\frac{1}{10},\frac{3}{5},\Lambda\,b(t)^{\frac{5}{3}}\right)$ is the Whittaker M function. The potential from which the Swift-Hohenberg PDE derives reads ($p = 1/3$):

$$\begin{aligned}\mathcal{F}\left[\beta(\mathbf{r},t)\right] = \int d\mathbf{r}\Big\{&\mathrm{M}\,\beta(\mathbf{r},t) \\ &+\left(\frac{\Gamma}{4}-\frac{\mathrm{K}}{2}\right)\beta(\mathbf{r},t)^2+\frac{1}{4}\,\beta(\mathbf{r},t)^4 \\ &-\frac{\Gamma}{4}\left[\left(\nabla^2+1\right)\beta(\mathbf{r},t)\right]^2\Big\}.\end{aligned} \quad \text{(A.9)}$$

At the critical point, it reduces to:

$$\begin{aligned}\mathcal{F}\left[\beta(\mathbf{r},t)\right] = \frac{1}{4}\int d\mathbf{r}\Big\{&\Gamma\beta(\mathbf{r},t)^2+\beta(\mathbf{r},t)^4 \\ &-\Gamma\left[\left(\nabla^2+1\right)\beta(\mathbf{r},t)\right]^2\Big\}.\end{aligned} \quad \text{(A.10)}$$

Appendix B. PDE approximation of vegetation spatio-temporal dynamics

B.1. *Approximation of uniform stationary states in the vicinity of the critical point*

Let $0 < \eta \ll 1$ be a smallness parameter that fixes the deviation of Λ from its critical value Λ_c given by (16). We set

$$\begin{aligned}\chi_c &= \chi_0 + \eta,\\ \chi_f &= \chi_c + \Lambda_c(1+\eta^2\,\kappa),\\ \mu &= \mu_c\left(1+\sum_i \eta^i \mu_i\right),\\ b_s &= b_c\,(1+\eta\,\beta_s)\,,\end{aligned} \tag{B.1}$$

replace these expressions in (14) and solve the equation obtained at each order in η. This yields:
Order η:

$$\mu_1 = 0. \tag{B.2}$$

Order η^2:

$$\mu_2 = \frac{2\,p}{1+2\,p}\,\kappa. \tag{B.3}$$

Order η^3:

$$\mathrm{M} = \beta_s(\mathrm{K}-\beta_s^2), \tag{B.4}$$

with

$$\mathrm{M} = \frac{3}{2}\frac{\mu_3}{p^2\,(1+2\,p)} \text{ and } \mathrm{K} = 3\,\frac{\kappa}{p\,(1+2\,p)}. \tag{B.5}$$

Eq. (B.4) is the equation of state for the excess stationary biomass density β_s.

B.2. *Swift-Hohenberg equation of vegetation*

To find a PDE approximation of Eq. (1), we expand this integro-differential logistic equation in terms of η as follows.
To begin with, let k^* be a finite (non-zero) Fourier mode that satisfies the conditions of marginal stability

$$\omega_{k^*} = 0 \quad \text{and} \quad \left(\frac{\partial\omega_k}{\partial k}\right)_{k=k^*} = 0. \tag{B.6}$$

For k^* to exist, the biomass "diffusion coefficient" must be small (in fact of order η or smaller). Hence, we put

$$\frac{\delta}{\sigma} = \eta D \tag{B.7}$$

and since, close to the critical point, the wavelength of a mode that satisfies (B.6) is much greater than L_a, we expand k^{*2} in terms of η:

$$k^{*2} = \eta\,k_0(1+\sum_i \eta^i\,k_i). \tag{B.8}$$

We set

$$b(\mathbf{r},t) = b_c\,(1+\eta\,\beta(\mathbf{r},t))\,, \tag{B.9}$$

replace the expressions (B.1-B.5) and (B.7-B.9) in (B.6). Up to $\mathcal{O}(\eta^2)$ the solution of the system of two equations obtained in this manner reads:
Order η:

$$\chi_0 = \Lambda_c\left(\frac{\varepsilon}{1-\varepsilon}\right), \tag{B.10}$$

$$k_0 = \frac{2}{5}\left(\frac{1+4\,p}{1+6\,p}\right)(1-\varepsilon)(1-\Delta) \tag{B.11}$$

with

$$\Delta = \frac{1}{3}D\,p\left(\frac{\varepsilon}{1-\varepsilon}\right)\left(\frac{\Lambda_c}{b_c}\right)^2\frac{e^{\left(-\frac{b_c}{1-\varepsilon}\right)}}{(1+4\,p)}. \tag{B.12}$$

Order η^2:

$$\beta_s = \pm\sqrt{\frac{1}{3}\left(\mathrm{K}-\frac{\Gamma}{2}\right)}, \tag{B.13}$$

$$k_1 = C_1 + C_2\,\beta + C_3\,\kappa, \tag{B.14}$$

with

$$\begin{aligned}\Gamma =& -\frac{9}{5}\frac{(1-\varepsilon)^2}{p\,\varepsilon\Lambda_c^2}\left[\frac{1+4\,p}{1+2\,p}\right]^2\frac{(1-\Delta)^2}{(1+6\,p)},\\ C1 =& \frac{b_c}{\Lambda_c}\left[\frac{\Delta}{1-\Delta} - \frac{(1+2\,p)(1-\varepsilon^2)}{2\,p\,\varepsilon}\right] + \\ & \frac{\Delta}{10}\frac{(1-\varepsilon)(1+4\,p)}{\sigma\,(1+6\,p)},\\ C2 =& -2\,p + \frac{\Delta}{1-\Delta}\left[1+2\,p\left(\frac{2-\varepsilon}{1-\varepsilon}\right)\right]\\ C3 =& -\frac{\Lambda_c\,\varepsilon}{(1-\varepsilon)(1-\Delta)}.\end{aligned} \tag{B.15}$$

Next, before expanding Eq. (1) in terms of η, we apply the transformation (23) to rescale its space and time units, we put $k_f = k^*$ and take expansion (B.8) into account. We then replace in (1) the expressions (B.1-B.5), (B.9-B.15) and the explicit expressions of $\mathcal{M}_f, \mathcal{M}_c$ and of the seed dispersion term. As a result, we find that up to terms of order η^2, Eq. (1) is automatically satisfied. At the order η^3,we find that

$$t^* = \frac{2}{3}\,p^2\exp\left(-\frac{b_c}{1-\varepsilon}\right), \tag{B.16}$$

and the Swift-Hohenberg equation (25), which is the functional derivative,

$$\partial_\tau\beta(\mathbf{r},t) = -\frac{\delta\mathcal{F}\,[\beta(\mathbf{r},t)]}{\delta\beta(\mathbf{r},t)}, \tag{B.17}$$

of the potential function (A.9). Thus, since

$$\frac{d\,\mathcal{F}\,[\beta(\tilde{\mathbf{r}},t)]}{dt} = -\left(\frac{\delta\mathcal{F}\,[\beta(\tilde{\mathbf{r}},t)]}{\delta\beta(\tilde{\mathbf{r}},t)}\right)^2 \leqq 0, \tag{B.18}$$

the dynamics is variational. $\mathcal{F}\,[\beta(\mathbf{r},t)]$ can only decreases in time till it reaches some minimum value compatible with the constraints. For $\mathrm{K} > 0$, the

stable and metastable states of the hysteresis loop correspond to the minima of the potential function. Their condition of coexistence reads

$$\beta_s = \pm\sqrt{\mathrm{K}}.$$

Acknowledgments
We thank John Wm Turner, Mustapha Tlidi and Vincent Deblauwe for helpful discussions. This work has benefited from a support granted by the European project ECOPAS.

References

Barbier, N., Couteron, P., Lejoly, J., Deblauwe, V., Lejeune, O., 2006. Self-organised vegetation patterning as fingerprint of climate and human impact on semiarid ecosystems. J. Ecology 94, 537-547.

Barbier, N., 2006. Interactions spatiales et auto-organisation des végétations semi-arides. PhD Thesis, Université Libre de Bruxelles.

Barbier, N., Couteron, P., Lefever, R., Deblauwe, V., Lejeune, O., 2008. Spatial decoupling of facilitation and competition at the origin of gap vegetation patterns in SW Niger. Ecology, 89, 1521-1531.

Bates, F. S., 1985. Polymer-Polymer phase behavior. Science, 251, 898-904.

Breshears, D. D., 2006. The grassland-forest continuum: trends in ecosystem properties for woody plant mosaics? Frontiers in Ecology and the Environment 4, 96-104.

Callaway, R. M., 1995. Positive interactions among plants. Botanical Rewiew, 61, 306-349.

Callaway, R. M., Walker, L.R., 1997. Competition and facilitation: a synthetic approach to interactions in plant communities. Ecology 78, 1958-1965.

Callaway, R. M., Brooker, R. W., Choler, P., Kikvidze, Z., Lortie, C. J., Michalet, R., Paolini,L., Pugnaire, F. I., Newingham, B., Aschehoug, E. T., Armas, C., Kikodze,D., Cook, B. J., 2002. Positive interactions among alpine plants increase with stress. Nature, 417, 844-848.

Callaway, R. M., Pennings, S. C. and Richards, C. L., 2003. Phenotypic plasticity and interactions among plants. Ecology 84, 1115-1128.

Cannas. S. A., Marco, D. E., Montemurro, M. A., 2006. Long range dispersal and spatial pattern formation in biological invasions. Math. Biosciences, 203, 155-170.

Couteron, P. and Lejeune, O., 2001. Periodic spotted patterns in semi-arid vegetation explained by a propagator-inhibition model. J. Ecology, 89, 616-628.

Couteron, P., 2002. Quantifying change in patterned semi-arid vegetation by Fourier analysis of digitized aerial photographs. Int. J. Remote Sensing, 23, 3407-3425.

Deblauwe, V., Barbier, N., Couteron, P., Lejeune, O., Bogaert, J., 2008. The global biogeography of semi-arid periodic vegetation patterns. Global Ecol. Biogeogr. DOI:10.1111:j.1466-8238.2008.00413.x.

D'Odorico, P., Laio, F., Ridolfi, L., 2006. Patterns as indicators of productivity enhancement by facilitation and competition in dryland vegetation. J. Geophys. Res. 111, G03010.

Gilad, E., von Hardenberg, J., Provenzale, A., Shachak, M., Meron, E., 2004. Ecosystems engineers: from pattern formation to habitat creation. Phys. Rev. Lett. 93, 098105,1-4.

In South-West Niger vegetated areas in non-banded (*i.e.* gapped or "diffuse") vegetation frequently display biomass densities of dry matter above 12t/ha while the figures for "bare" gaps are generally less than 0.5 t/ha. See, Hiernaux, P., Gérard, B., 1999. The influence of vegetation pattern on the productivity, diversity and stability of vegetation: The case of the *brousse tigrée* in the Sahel. Acta Oecol. 20, 147-158.

Hilali, M'F., Dewel, G., Borckmans, P.,1996. Subharmonic and strong resonances through coupling with a zero mode. Phys. Lett. A 217, 263-268.

HilleRisLambers, R., Rietkerk, M., van den Bosch, F., Prins, H. H. T., de Kroon, H., 2001. Vegetation pattern formation in semi-arid grazing systems. Ecology 82, 50-61.

Kéfi, S., Rietkerk, M., van Baalen, M., Loreau, M., 2007. Local facilitation, bistability and transitions in arid ecosystems. Theoret. Pop. Biol. 71,367-379.

Kéfi, D., 2008. *Reading the signs - Spatial vegetation patterns, arid ecosystems and desertification,* Gildeprint Drukkerijen BV, Enschede.

Klausmeier, C. A., 1999. Regular and irregular patterns in semiarid vegetation. Science, 284,1826-1828.

Korteweg, D. J., 1891. Sur les points de plissement. Arch. nerl. 24, 57-98 (french translation from Korteweg's original paper in german (1889)).

Langer, J. S., 1991. An introduction to the kinetics of first-order phase transitions. In: *Solids far*

from equilibrium. 297-363. Ed. C. Godrèche. Cambridge University Press.

Lefever, R., Lejeune, O., 1997. On the origin of tiger bush. Bull. Math. Biol. 59, 263-294.

Lefever, R., Lejeune, O., Couteron, P., 2000. Generic modelling of vegetation patterns. A case study of tiger bush in sub-saharian sahel. In: *Mathematical Models for Biological Pattern Formation: frontiers in biological mathematics* (eds Othmer, H., Maini, P. K.), IMA Volumes in Mathematics and its Applications, Frontiers in Applied Mathematics, Series 121. Springer-Verlag.

Leibler, L., 1980. Theory of microphase separation in block copolymers. Macromolecules, 13, 1602-1617.

Lejeune, O., Couteron, P., Lefever, R., 1999. Short range cooperativity competing with long range inhibition explains vegetation patterns. Acta Oecologica 20, 171-183; Lejeune, O., Tlidi, M., 1999. A model for the explanation of vegetation stripes (tiger bush). J. Vegetation Science, 10, 201-208.

Lejeune, O., Tlidi, M., Lefever, R., 2004. Vegetation spots and stripes: dissipative structures in arid landscapes. Int. J. Quantum Chemistry 98, 261-271.

Ludwig, J. A., Wilcox, B. P., Breshears, D. D., Tongway, D. J., Imeson, A. C., 2005. Vegetation patches and runoff-erosion as interacting ecohydrological processes in semiarid landscapes. Ecology 86, 288-297.

Maruvka, Y. E., Shnerb, N. M., 2006. Nonlocal competition and logistic growth: Patterns, defects, and fronts. Phys. Rev. E 73, 038101-1-4.

Meron, E., Yizhaq, H., Gilad, E., 2007. Localized structures in dryland vegetation: forms and function. Chaos 17, 037109.

Okayasu, T., Aizawa, Y. 2001. Systematic analysis of periodic vegetation patterns. Prog. Theor. Phys. 106, 705-719.

Pomeau, Y., and Manneville, P., 1980. Wavelength selection in cellular flows. Phys. Lett. 75A, 296-298.

Rietkerk, M., Dekker, S. C., de Ruiter, P. C., van de Koppel, J., 2004. Self-organized patchiness and catastrophic shifts in ecosystems. Science 305, 1926-1929.

Sheffer, E., Yizhaq, H., Gilad, E., Shachak, M., Meron, E., 2007. Why do plants in resource-deprived environments form rings? Ecological Complexity 4, 192-200.

Schenk, H. J., Jackson, R. B., 2002. Rooting depths, lateral root spreads and below-ground/above-ground allometries of plants in water-limited ecosystems. J. Ecology 90, 480-494.

Schlesinger, W. H., Reynolds, J. F., Cunninghamm, G. L., Huenneke, L. F., Jarrel, W. M., Virginia, R. A., Whitford, W. G., 1990. Biological feedback in global desertification. Science 247, 1043-1048.

Sherratt, J. A., 2005. An analysis of vegetation stripe formation in semi-arid landscapes. J. Math. Biol. 51, 183-197.

Shnerb, N. M. Sarah, P., Lavee, H., Solomon, S., 2003. Reactive glass and vegetation patterns. Phys. Rev. Lett. 90, 011903-1-12.

Swift, J. B., Hohenberg, P. C., 1977. Hydrodynamic fluctuations at the convective instability. Phys. Rev A 15, 319-328.

Tlidi, M., Mandel, P., Lefever, R., 1998. Kinetics of localized pattern formation in optical systems. Phys. Rev. Lett. 81, 979-982.

Tlidi, M., Lefever, R., Vladimirov, A., 2008. On vegetation clustering, localized bare soil spots and fairy circles. Lect. Notes Phys. 751, 381-402.

Tongway, D. J., Valentin, C., Seghieri, J., Eds, 2001. *Banded vegetation patterning in arid and semiarid environments*, Springer-Verlag, New York.

Ursino, N., 2005. The influence of soil properties on the formation of unstable vegetation patterns on hillsides of semiarid catchments. Adv. Water Resour. 28, 956-963.

Valentin, C., Poesen, J., Eds, 1999. *The significance of Soil, Water and Landscape Processes in Banded Vegetation Patterning.* Catena, Special Issue 37.

von Hardenberg, J., Meron, E., Shachak, M., Zarmi, Y., 2001. Diversity of vegetation patterns and desertification. Phys. Rev. Lett. 87, 198101-1-4.

Wilcox, B. P., Breshears, D. D., Allen, C. D., 2003. Ecohydrology of a resource-conserving semiarid woodland: effects of scale and disturbance. Ecological Monographs 73, 223-239.

Zeng, X., Shen, S. S. P., Zeng, X., Dickinson, R., 2004. Multiple equilibrium states and the abrupt transitions in a dynamical system of soil water interacting with vegetation. Geophys. Res. Lett. 31, L05501-5.